NANOCONFINED CALCITE GROWTH IN SITU
Microfluidic Channel, Growth rims, Cavity, Crystallation pressure and Disjoining pressure

by

Lei Li

THESIS

for the degree of

Philosophiae Doctor

Prepared under joint supervision from the

Faculty of Mathematics and Natural Sciences

University of Oslo

September 2018

Series of dissertations submitted to the
Faculty of Mathematics and Natural Sciences, University of Oslo
No. 2094

ISSN 1501-7710

Cover: Hanne Baadsgaard Utigard.
Print production: Reprosentralen, University of Oslo.

Contents

CHAPTER 1

Introduction

1.1 Motivation

Calcium Carbonate($CaCO_3$) is a common substance on earth. It is the main component of pearls, snails, eggs, shells of marine organisms, animal skeletons etc.[26]. $CaCO_3$ has three stable polymorphs: calcite, vaterite and aragonite. Calcite is the most stable polymorph[22]. Aragonite will change to calcite over timescales of days and vaterite is even less stable[27]. In this thesis, I will focus on the most stable polymorph of $CaCO_3$, i.e., calcite.

During the long history of earth development, the organisms with calcium carbonate skeletons sediment to the sea floor. The sediments undergo compaction, where dissolution and recrystallization of calcite occur to form limestone. Some of the carbonate rocks are buried deeper and undergo another recrystallization and emerge as marble[12]. As shown in the example illustrated in Figure 1.1, both limestone and marble are used for construction and sculptures since 3000 years ago. They are the gems of human being's history. However, how to protect them from weathering and deterioration is a huge problem to us now. Salt recrystallization in the stone pore space plays an important role during the weathering process. It could break the stone, grow fractures and enlarge the weathering surface[10]. Even in Portland cement, CO_2 is slowly adsorbed from air, and calcite is crystallized inside cement, where the fractures start[2]. The crystallization of calcite in other environments has also been shown to create forces that break other mineral grains[20] and lift rock overburden[11]. An interesting question is how much pressure could one single crystal generate during its growth?

In 1853, Lavalle first reported the work generated by growing crystals[15]. He found that crystals growing from supersaturated solutions were able to push themselves upwards. Later, Becker and Day demonstrated that centimeter sized growing crystals can lift an one kilogram block over a distance of millimeters[1]. Taber presented similar results[23]. However, Taber et. al found that the confined crystal surface becames really rough, which means that it is impossible to measure the contact area and thus to calculate the pressure during crystal growth. Until 1949, the only quantitative measurements were made by Correns and Steinborn, who found an agreement with their derived equation for equilibrium crystallization pressure[4]. However, their results have pointed out that Correns' equation is off by almost a factor of two due to neglecting the number of ions in the dissolved salt and the effects of non-ideality[9].

Figure 1.1: The weathering of Parthenon Temple.

Becker and Day failed to measure the contact area of confined growing crystals. Now, we have methods like reflection interference contrast microscopy(RICM), which allow us to measure the contact area during crystal growth. In addition, a microfluidic chip is used to study calcite growth. This allows us to minimize the effect of convection, diffusion and turbulence on the concentration, which means the calcite is growing under stable supersaturation and boundary conditions.

CHAPTER 2

Stress generation due to crystal growth

Crystallization is the process of forming a highly structured solid from a solution or melt. The driving force for crystallization depends on several parameters, e.g., subcooling (for melt), supersaturation (for solutions), temperature (for example : ice), surface normal stress. In this chapter, I will focus on the crystallization from solutions which is the most common situation in weathering process. A saturated solution is a solution in which no more solute can be dissolved in the solvent. A supersaturated solution can be obtained from saturated solution by, e.g., evaporation, temperature change or pH change. If the crystallization happens in a fracture or a pore, the crystal will perform mechanical work by 'pushing' on the surrounding matrix. Then, the crystal may wedge itself into rocks to propagate fractures and produce damage through frost heave and salt weathering. The stresses generated on the surrounding matrix are often referred to 'the forces of crystallization' or 'crystallization pressure'.

2.1 Experiments of crystallization pressure

The crystallization pressure has been studied for many years. It was first reported by Lavalle in 1853[15]. He noted that the growing crystal could pushes itself upwards. The experiment definitely showed the work done by growing crystal. But, it didn't give a quantitative measurement of crystallization pressure. Fifty years later, Becker and Day designed their experiment to measure the crystallization pressure[1] (see Figure 2.1). A 1 cm well-formed alum crystal was placed between two glass plates. A 1 kg block was placed on the top of the glass plate. The whole setup was put in an ordinary crystallizing dish. A saturated solution of alum was poured into the crystallizing dish in sufficient quantity to cover the whole crystal. The experiment was free from temperature changes and dust. After several hours, they found the crystal grew and the weight was pushed 0.5 mm upwards due to the slow evaporation. The crystal succeeded in lifting (I) its own weight, (II) the weight of the top glass plate, (III) the weight of the load upon the top glass plate. They also succeeded with different crystal as copper sulphate, potassium ferrocyanide, lead nitrate. Their experiment showed clearly that the crystallization pressure was exerted to separate the open walls during the crystal growth. However, an unexpected difficulty was encountered when they calculated the

pressure at the growing interface lifting the weight. A hollow formed below the crystal during its growth. So that 'the measurement of the contact area thus recorded is a matter of great difficulty and uncertainty, and the force per unit area which the crystal exert is, therefore, hard to estimate.'[1]. They experienced issues when trying to measure the contact area during the crystal growth. But, they still predicted that the contact area 'changes constantly as the crystals grow, and is less for a smaller load than for a larger one'. They also measured the upper crystal surface and found that the upper surface was much more flat than the lower surface.

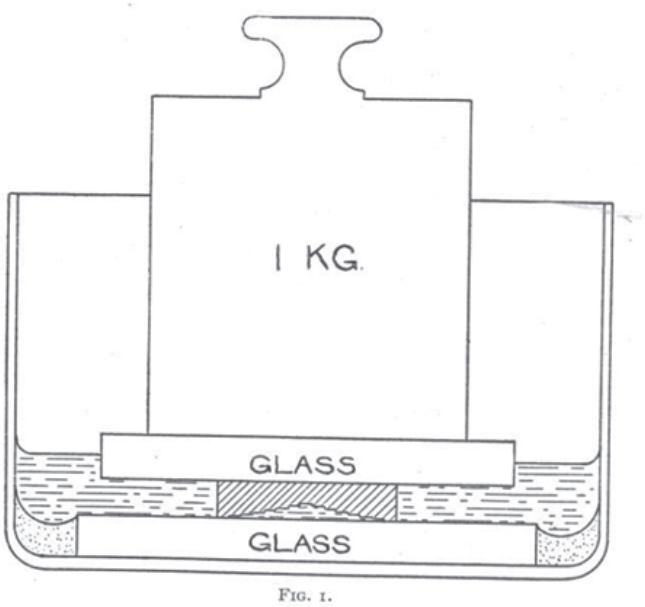

FIG. 1.

Figure 2.1: Experiment setup used by Becker and Day. A 1 cm wide alum crystal was placed between two glass plates. On the top glass, a 1 kg block was loaded. The whole crystal was immersed in a saturated alum solution. Due to the slow evaporation of H_2O, the solution became supersaturated, and the alum crystal grew.

In 1949, Correns managed to solve the problem of crystallization pressure and the crystal dissolution under pressure. Where B is the loaded force, h is the distance pushed by crystal, n is the molality of the solution, T is the temperature, R is the ideal gas constant, p is the osmotic pressure and p_s is the osmotic pressure in a saturated solution.

$$A_1 = Bh. \tag{2.1}$$

$$A_2 = nRTln(p/p_s). \tag{2.2}$$

According to the principle of maximum work A_1=A_2. So we have,

$$Bh = nRTln(p/p_s). \tag{2.3}$$

If we use B=Ps. where P is the pressure on the crystal and s is the contact area. The above equation therefore changes to

$$Pv_c = RTln(p/p_s), \tag{2.4}$$

where v_c is the molar volume of the crystalline substance. In addition, we can replace the osmotic pressure with the solute concentration.

$$Pv_c = RTln(c/c_s). \tag{2.5}$$

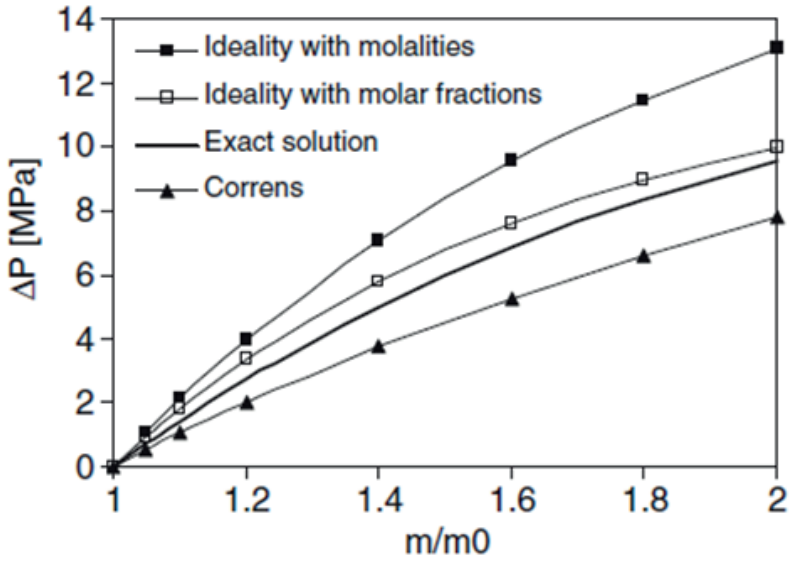

Figure 2.2: Correns' crystallization pressure vs the solution's supersaturation.

As in figure 2.2, the crystallization pressure P in equation 2.5 is the maximum pressure that can be exceeded when the crystal grows in a solution with concentration c. If the crystal experiences a pressure larger than this maximum value, the crystal can not grow, it even starts to dissolve. Correns used the phase-boundary force to explain this phenomenon. Only when the crystal-substance phase boundary force is larger than the sum of solution-substance and the crystal-solution phase boundary force, the solution can enter the space between the crystal and substance. This allows the crystal to grow at the confined interface. But Correns also mentioned that some experimental result showed that the crystal stops to grow under suitable pressure.

In recent years, plenty of experiments has been done to measure the crystal growth pressure under confinement. K. Sekine et.al. observed a Halite growth in the PDMS channel. The PDMS wall was deformed when the halite grew against it. A maximum value of 2 Mpa pressure was estimated at the crystal corner[21]. Julie Dedsarnaud et.al. performed a new experiment of loaded KCl crystal growth under strictly pressure controlled. They found that the loaded crystal surface dissolved slightly and grew on the unloaded faces, due to the change of the supersaturation. And also they declared that the crystal is not able to grow against the applied pressure which contradict Corrrens conclusions[6]. J Desarnaud et.al. carried out a NaCl and KCl crystal growth on the hydrophilic and hydrophobic glass walls. The experiments revealed the importance of confined liquid film in the confined crystal growth[7]. A Naillon et.al reanounced theimportance of the confined liquid film during the crystal growth in the pores[17].

2.2 Confined solution film and disjoining pressure

In order to grow on the loaded crystal surface, there must be a liquid film between the crystal and substance present. If the film disappears, the material can not diffuse to the confined crystal surface. (solid diffusion is too slow to grow the loaded crystal surface.) Normally, the thickness of the film is less than 100 nm. In a crystal-solution-substance system, the disjoining pressure is the key to keep the confined solution film. The disjoining pressure can be derived from a macroscopic continuum picture by considering the interfacial energy of solid-liquid and solid-solid interfaces or a microscopic continuum model, where the interaction forces between two solid surface separated by a liquid solution are considered. When a solid surface is put in a solution, its surfaces get charged due to the ions in the solution. As illustrated in Figure 2.3, the water molecules and ions in the stern layer are bound to the solid surface (The Stern Layer is the first (internal) layer of the electric double layer, which forms at a charged surface in an ionic solution.). The ions are balanced by an oppositely charged region referred to as counter ions. Thus, an electrical double layer is formed on the solid-solution interface. The inner region of the double layer includes ions bound relatively tightly to the solid. In the outer region, the balance of electrostatic forces and random thermal motion determines the ion distribution. Therefore, the potential in this region decays with the increasing distance from the surface. In Figure 2.4, the zeta potential is shown.

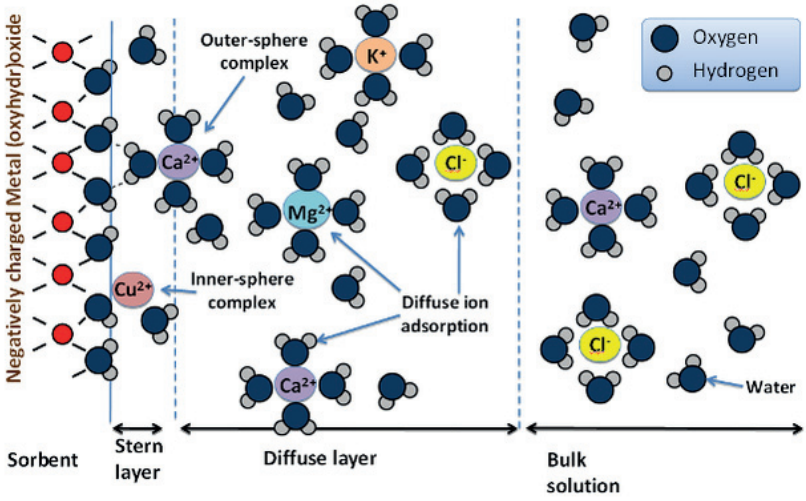

Figure 2.3: The solid surface in the water solution. Figure:https://en.wikipedia.org/wiki/Doublelayer

When the solid and crystal surface are close enough to each other, the interaction of the surface electric double layer contributes to the disjoining pressure. The interaction energy U_D related to this process depends exponentially on the separation distance and ions concentration [13].

$$U_{DL}(r) = 4\pi\epsilon\psi^2 exp(-kr)/2 + r, \tag{2.6}$$

where ϵ is the dielectric constant of the liquid medium, ψ is the electrical potential on the solid surface, k is known as the Debye-huckel constant and r is the distance to the solid surface. Another part of disjoining pressure comes from the long range Van der Waals force. The non-retarded Van der Waals interaction energy between the solid and calcite surface follows the dependence[13],

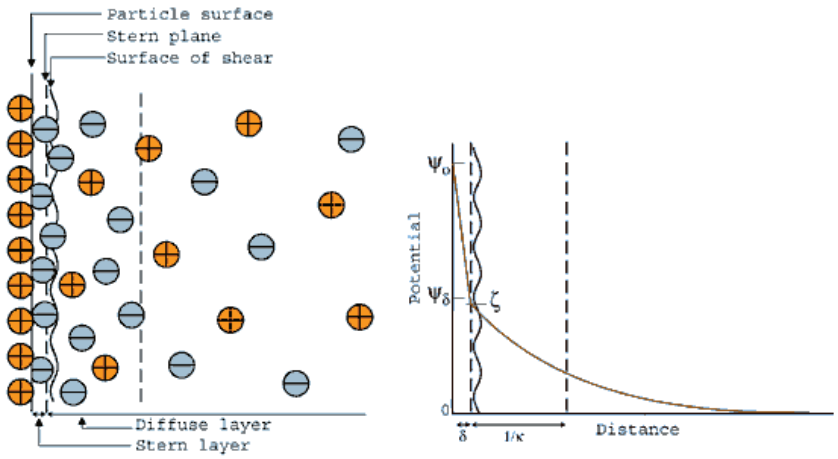

Figure 2.4: The zeta potential on the solid surface. Figure:https://www.brookhaveninstruments.com/what-is-zeta-potential

$$U_{vdW}(r) = -A/12\pi h^2. \tag{2.7}$$

Where A is Hamaker constant, r is the distance between the solid to the crystal surface. Here, the Hamaker constant is typically positive, which means the van der Waals force is attractive and increasing with closing distance.

The combination of U_{DL} and U_{vdW} is called DLVO theory, named after Derjaguin and Landau[5] and Verwey and Overbeek [25]. Figure 2.5 shows the competition between van der Waals and electric double layer energy. It provides a good quantitative understanding of the repulsive force between a solid and a crystal surface in solution.

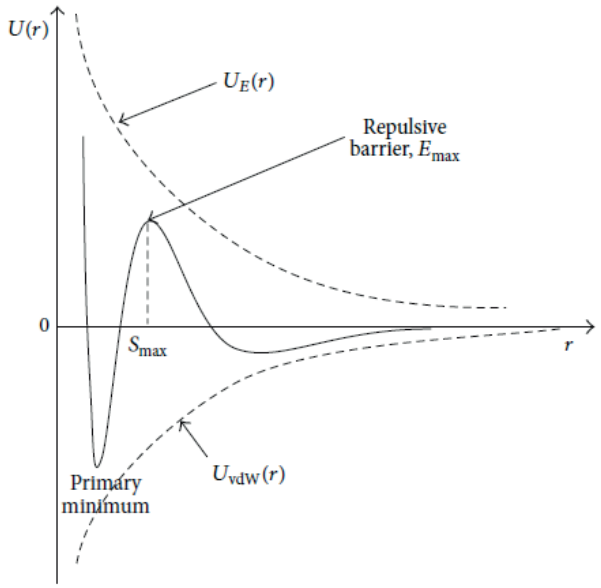

Figure 2.5: The interaction energy vs distance by DLVO theory.

The DLVO theory is very important for the understanding of disjoining pressure. But, there is also a non-DLVO force, i.e., the hydration force, which is important when the solid-crystal surface reaches distances of a few water molecule layers. In

this case, the water molecule layers become structured in the confined liquid film. In the calcite-glass confined film, the disjoining pressure increases quite fast when there are only a few water molecule layers left. To understand the disjoining pressure in calcite-glass confined film, experimental measurements are necessary. Typically, it is measured by a surface forces apparatus[14] or atomic force microscopy[8]. Thanks to Diao's work[8], we fitted the disjoining pressure in calcite-glass confined film as a function of distance(see Figure 2.6).

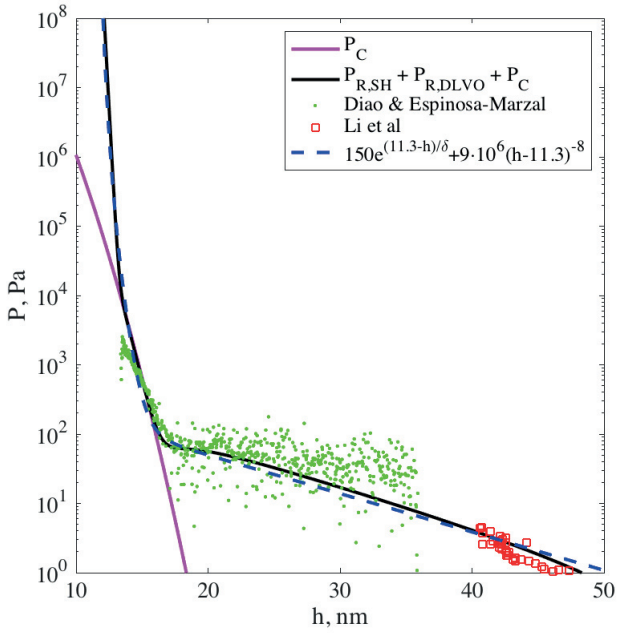

Figure 2.6: The disjoining pressure in the calcite-glass confined film as a function of distance. The red dots are from my experiment. The green dots are from Diao's AFM measurement[8]. The disjoinning pressure is fit with blue line.

2.3 Diffusion, mass balance and force balance

Correns pointed out that the confined solution film is really important to transport the ions and grow the confined crystal surface. Here, I will discuss the diffusion in the confined film. The diffusion of ions in the confined film is described by Fick's law.

$$J_m = -D(dc/dx). \tag{2.8}$$

J_m is the mass flux, D is the diffusion coefficient, c is the concentration and x is the distance between crystal and confining interface. In bulk solution, D is a constant. But, if the confined film is extremely thin, which means the ions have to diffuse in the stern layer, D is not a constant any more. In 2017, Mutisya presented their result about water diffusion in calcite slit pores[16], which shows that the diffusion constant decreases a lot when the confined film reaches 1 nm. Figure 2.8 Since the ions in water solution is hydrated, their effective diameter is much larger than water molecule. We estimate that the diffusion constant of ions in narrow confined film is even much smaller. When the calcite is pushed extremely close to the cover glass, the growth

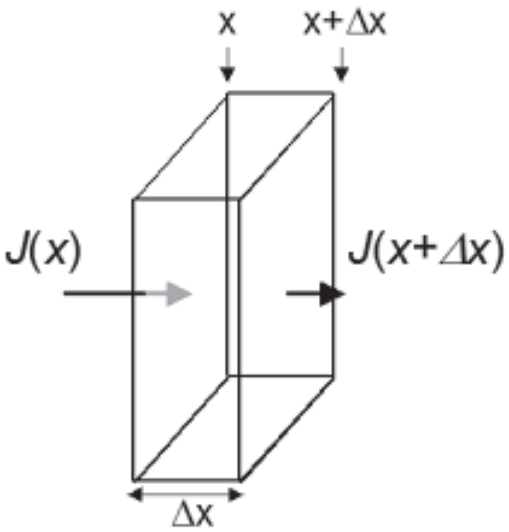

Figure 2.7: The ions diffusion in the solution.

of confined surface is really slow due to the thin confined film and the decay of the diffusion constant. In the experiments described in this thesis, the confined film is larger than 10nm. Therefore, we will use the diffusion constant as it is in the bulk solution.

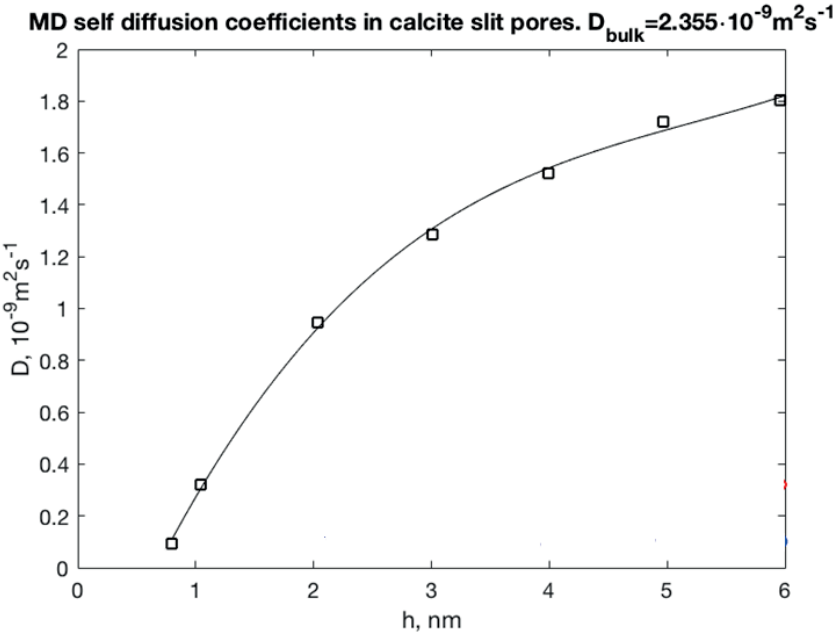

Figure 2.8: The relationship between diffusion constant and the thickness of confined film[16].

Becker and Day found that the confined crystal surface is cup-shaped. So, we can simplify the confined crystal surface as shown in Figure 2.9. The size of the crystal is L×L, the width of the contact area is w. The concentration outside of the crystal is c, and the concentration in the cavity is c_0. Here, the crystal surface stopped to grow.

Since the crystal surface is confined, all of the ions used to grow the contact area have to diffuse from the bulk solution. That is the mass balance. Here, we have the

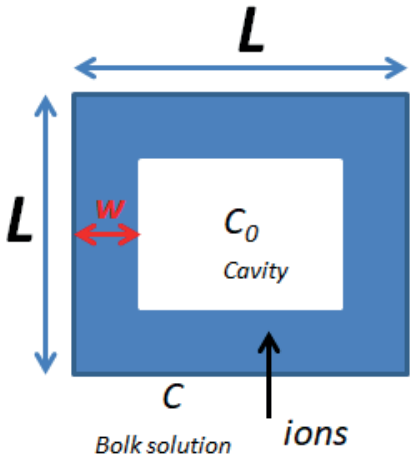

Figure 2.9: The simplified confined crystal surface.

mass of the ions, which diffused into the confined liquid film.

$$m = J_m x L M t. \tag{2.9}$$

where $J_m = -D(c_0 - c)/w$ is the mass flux, x is the thickness of confined film, M is the crystal molar mass and t is the time. The mass, which enters the confined liquid film by diffusion should equal to the mass grown on the crystal.

$$m = J_m x L M t = \rho V_z t(Lw - 4w^2). \tag{2.10}$$

Thus, we have combined the growth rate on the confined surface to the concentration c. The relationship between the thickness of confined film x and the disjoinning pressure P(x) is shown in Figure 2.6. Then, we have force balance as,

$$F = P(x)(Lw - 4w^2), \tag{2.11}$$

where F is the loaded force on the crystal. In Becker and Day's experiment, F is the sum of (I) its own weight, (II) the weight of the top glass plate, (III) the weight of the load upon the top glass plate. Of course, we have to deduct the buoyancy.

CHAPTER 3

Experiment

3.1 Reflection Interference Contrast Microscopy

Since the confined crystal surface becomes rough during its growth, Becker and Day have carefully explained the difficulty of measuring the contact area of confined crystal surface[1]. They failed to measure the contact area during the crystal growth. They leave us a prediction that the contact area changes constantly as the crystal grow, and is less for a smaller load than for a larger one. In this thesis, we reported high resolution measurements of the topography of the confined crystal surface while it grows. The measurements were performed by reflection interference contrast microscopy (RICM). The basic principle of RICM is illustrated in Figure 3.1. The incident LED light from the microscope is reflected both from the crytal-water interface and from the glass-water interface. Thus, a part:

$$I_r \propto E_g^2 + E_c^2 + E_g E_c \cos(4\pi hn/\lambda + \pi) \tag{3.1}$$

of the total intensity $I_{det} = I_0 + I_r$ reaching the detector is given by the interference of these two reflected parts of the incident light. Here, E_g is the electromagnetic wave amplitude of the light reflected at the glass-water interface, E_c is the electromagnetic wave amplitude of the light reflected at the crystal-water interface, λ=550 nm is the wavelength of the light, h is the distance between the glass and the crystal and n=1.33 is the refractive index of water. I_0 denotes the part of the light reaching the detector by scattering at other interfaces of the system. Here, the light is represented by its central beam. Effects of the finite aperture of the imaging systems are not considered.

The reflected interference contrast can be achieved with almost any microscope using reflected light illumination. The contrast (I_r/I_0) can be augmented by using specialized objectives with a $\lambda/4$ retarder[19]. However, in this study we have used ordinary objectives (Olympus UPLanFLN 100x/1.30 and Olympus UPLanFI 40x/0.75p) mounted on an Olympus GX71 inverted microscope with a blue LED light source. Images were recorded with a Pointgrey camera (Mono, Grasshopper3, GS3-U3-91S6M-C) with 3376x2704 resolution and saved as 8 bit TIFF files. The image sequences are analyzed by in-house developed scripts in Matlab and ImageJ.

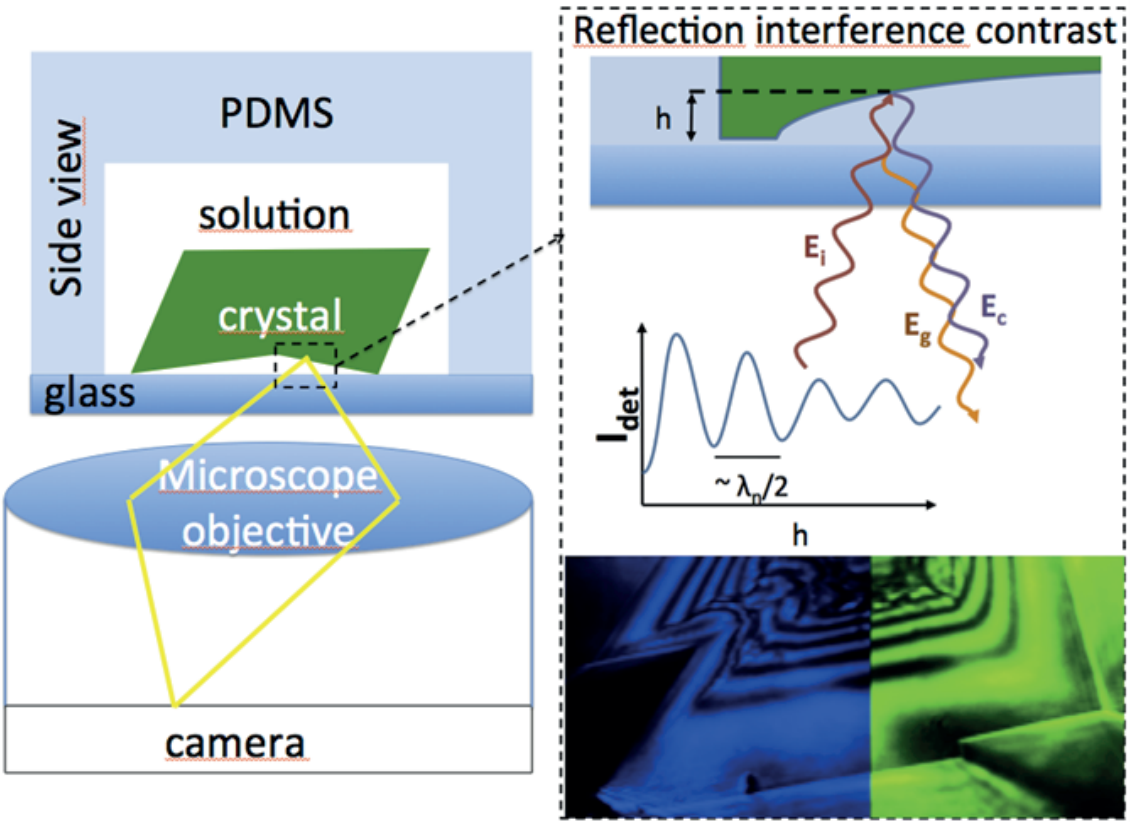

Figure 3.1: Principle of RICM. The crystal is illuminated from the bottom, which is illustrated here by the electric field, E_i, of the incident light. Due to the interference of the light reflected by the crystal-water interface, E_c, with the light reflected by the glass-water interface, E_g, the detected intensity, I_{det}, depends on the distance, h, between the two interfaces and on the wavelength of the light,λ. Exemplary RICM images of a calcite crystal using a blue LED (left half) and a green LED (right half) are shown at the bottom. The fringes align at the outer part (rim) of the crystal, but differ for larger distances h towards the central part of the confined interface.

3.2 Microfluidic channel and flow stability

In Becker and Day's experiment, the crystal was growing due to the supersaturation generated by the evaporation of the solution. But they didn't control the boundary condition of crystal growth. The ions' concentration around the crystal could have varied due to convection or turbulence in the solution, which may have been caused by the concentration difference in the solution, shaking of the setup or air flow on the solutions surface. In the experiments described in this thesis, we used microfluidic channels to grow crystals, which allowed us to: (I) nucleate calcium carbonate crystals in a limited area that permits imaging access. (II) remove other polymorphs than calcite. (III) control stable saturation conditions at the growing crystal surface. (IV) permit slow growth of rhombohedral crystals from the nuclei. (V) get rid of dust during the calcite growth.

3.2.1 Microfluidic channel

The purpose of this work was to grow calcite in the microfluidic channel, I designed a channel as Figure 3.2, which has three inlets and one outlet. The inlets are for calcium chloride solution, water and sodium carbonate. When the solutions start to flow in the channel, calcium and carbonate ions diffuse into the water and precipitate there. By changing the ratio of the water, calcium chloride and sodium carbonate solution flow rate, we can control the concentration of calcium carbonate in the channel. By increasing the flow rate of calcium chloride and sodium carbonate solution, the concentration of calcium carbonate increases in the channel. When calcium carbonate gets supersaturated in the channel, the nucleation starts. Then, the nuclei grows bigger and bigger and finally attachs to the cover glass. We could find the nucleated crystal by microscopy. Then, I reduce the flow rate of calcium chloride and sodium carbonate solution, in a way that the solution becomes supersaturated to a metastable amount at the place of the nuclei. Metastable solution means that the ions concentration is high enough to grow the nucleated crystal, but not enough for nucleation. By varying the ions concentration, the growth rate of the crystal can be controlled.

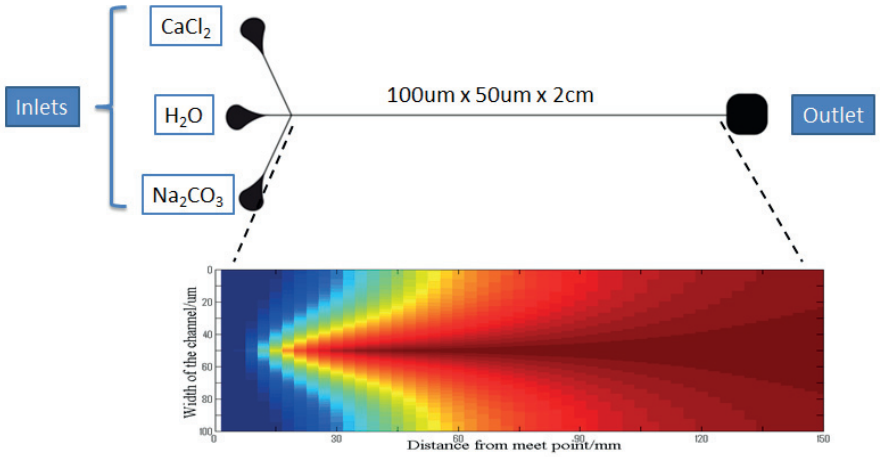

Figure 3.2: Top: The pattern of microfluidic channel.(up) The channel was designed with three inlets and one outlet. The upper-inlet is for calcium chloride solution, the middle-inlet is for water, the lower-inlet is for sodium carbonate solution. Bottom: After the junction of the inlets, calcium and carbonate ions diffuse towards to each other and precipitate calcium carbonate. The lower image is showing the concentration of calcium carbonate in the channel due to the ions diffusion.

The designed pattern is sent to Selba S.A (www.selba.ch) where it is printed on a transparent film. The film is used for photolithography. The photolithography protocol in our lab is shown below,

- Turn on the hot plate, set the temperature as 150 °C.
- Clean the wafer with Acetone and Isopropanol, remove the liquid with N_2 air gun.
- Dry the wafer on the hot plate at 150 °C for 10 minutes. Then put the wafer on the spin

- Pore the SU-8 GM1070 photoresist from Gersteltec (www.gersteltec.ch) on the wafer, try to avoid bubbles. Set the spin speed as 2000rpm for 40 seconds. Acceleration is 100rpm/s. Relax the wafer on the spin for 10 minutes after the centrifugation.

- Put the wafer on the hot plate for prebake. 15 minutes at 65°C, 35 minutes at 95°C. The temperature raises at 2°C/min.

- Put the wafer in the UV-KUB2 exposure holder. Put the pattern on the wafer (print side towards the wafer). Clean the cover glass and put it on the pattern. Set the thickness as 500 μm. Radiate the wafer.

- Relax the wafer for 10 minutes. Post bake: 15 minutes at 65°C, 40 minutes at 95°C. 2°C/min.

- Put the wafer in PGMEA for developing 3 minutes. Then rinse with isopropanol. Dry it with nitrogen air gun.

- Hard bake: 135°C for 2 hours

The channel networks were cast in PDMS (DC sylgard-184A) in 1:10 ratio of elastomer to curing agent, 1.5mm diameter holes punched for inlets and outlets. The PDMS and VWR cover glass were plasma treated (Electro-Technic Model BD-20V) before assembly. Flow rate was controlled using a syringe pump (Kd Scientific legato 180, USA) with Halmiton glass syringes (Halmiton 1000 syringe series, Halmiton company, VWR)) and an Elveflow system (Elveflow OB1 mk3, France). The channels, which have been used most in this study were 120 μm wide and 45 μm high, the distance from the inlet to the imaging site was 10-50 mm and the flow rates during the growth was in the range 0.2-1 μl/min.

3.2.2 flow stability

Since the calcium carbonate concentration in the channel is controlled by the fluid flow rates, the flow stability is extremely important to achieve the stable concentrations necessary for crystal growth. First, the flow stability in the microfluidic channel has been tested. Therefore, we pumped water, methylene blue solution and water into the three inlets. The stability of the syringe pump and gas pressure control systems have been separately tested as shown in Figure 3.4. The gas pressure control system includes an Elveflow controller (Elveflow OB1 mk3, www.elveflow.com), which has both a flow rate and a pressure control mode, it includes flow valves (Elveflow MUX) and flow sensors (0.4-7 μL/min, Elveflow). The input pressures P_i are controlled by the OB1. The three inlets have the same flow resistance so that the pressure control mode is achieved by setting the same inlet pressures $P_1 = P_2 = P_3$. In flow rate mode, OB1 adjusts the pressure to keep each flow rate constant. The syringe pump system includes a syringe pump (KD Scientific legato 180, www.kdscientific.com), BD plastic syringe (BD science, www.bd.com), Halmiton glass syringe (Halmiton 1000 syringe series, www.hamiltoncompany.com), flow valve (Elveflow MUX) and flow sensors (0.4-7 μL/min, Elveflow). The flow rate is controlled by the speed of the plunger and the inner diameter of the syringe. Because the accuracy of the syringe diameters of plastic and glass syringes differ, we tested their stability separately. Figure 3.5 displays the configurations used to test the flow stability: water was injected into the channel

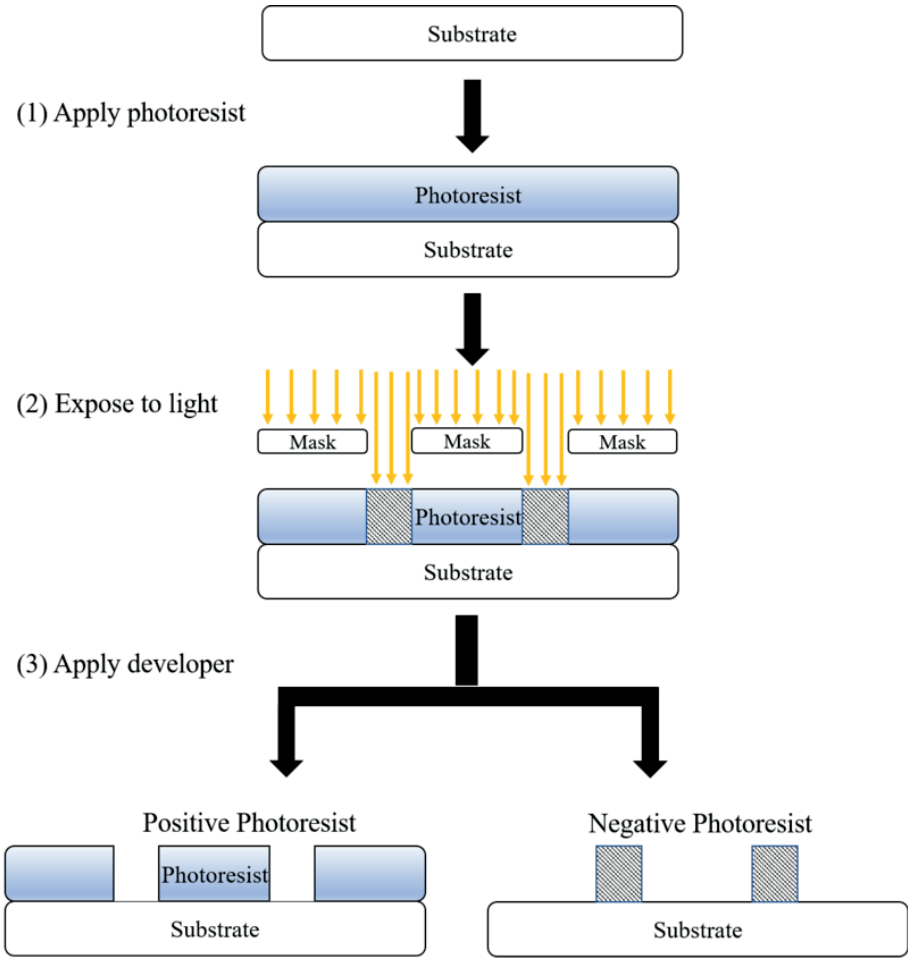

Figure 3.3: The process of photolithography. Basically, the process has three steps: (I) apply the photoresist. (II) expose to UV light. (III) apply the developer. the pattern is on the wafer now.

from inlets 1 and 3 with the flow rates φ_1 and φ_3 and methylene-blue solution (CAS Number: 61-73-4, Aldon Corp www.aldon-chem.com) was injected through inlet 2 at flow rate φ_2 which created two water/methylene-blue interfaces. Images of the flows (see Figures 3.5) have been recorded for 5 hours. By averaging the intensity of the image along Y direction, we plotted the averaged intensity I_m along X direction (Figure 3.5A). The channel edges x_1 and x_2 and the interface of the water/methylene blue were clearly identified by thresholding (see red lines in Figure 3.5A). The relative volume of water in the channel γ was used to study the flow stability:

$$\gamma = \frac{\bar{I_m}}{\bar{I_w}} = \frac{\int_{x_1}^{x_2} I_m dx}{\int_{x_1}^{x_2} I_w dx}, \tag{3.2}$$

where $\bar{I_m}$ is the average image intensity of the water/methylene-blue/water solution in the channel (Figure 3.5A black line). And $\bar{I_w}$ means the average image intensity when there is only water in the channel (Figure 3.5A blue line) and x_1 and x_2 are the edges of the channel (Figure 3.5A red lines).

The stability of the $CaCO_3$ concentration, c, which is proportional to the volume fraction in the flow is key to accurate and reliable measurements of crystal growth rates. The flow stability tests were performed for 5 hours with 2 water input channels

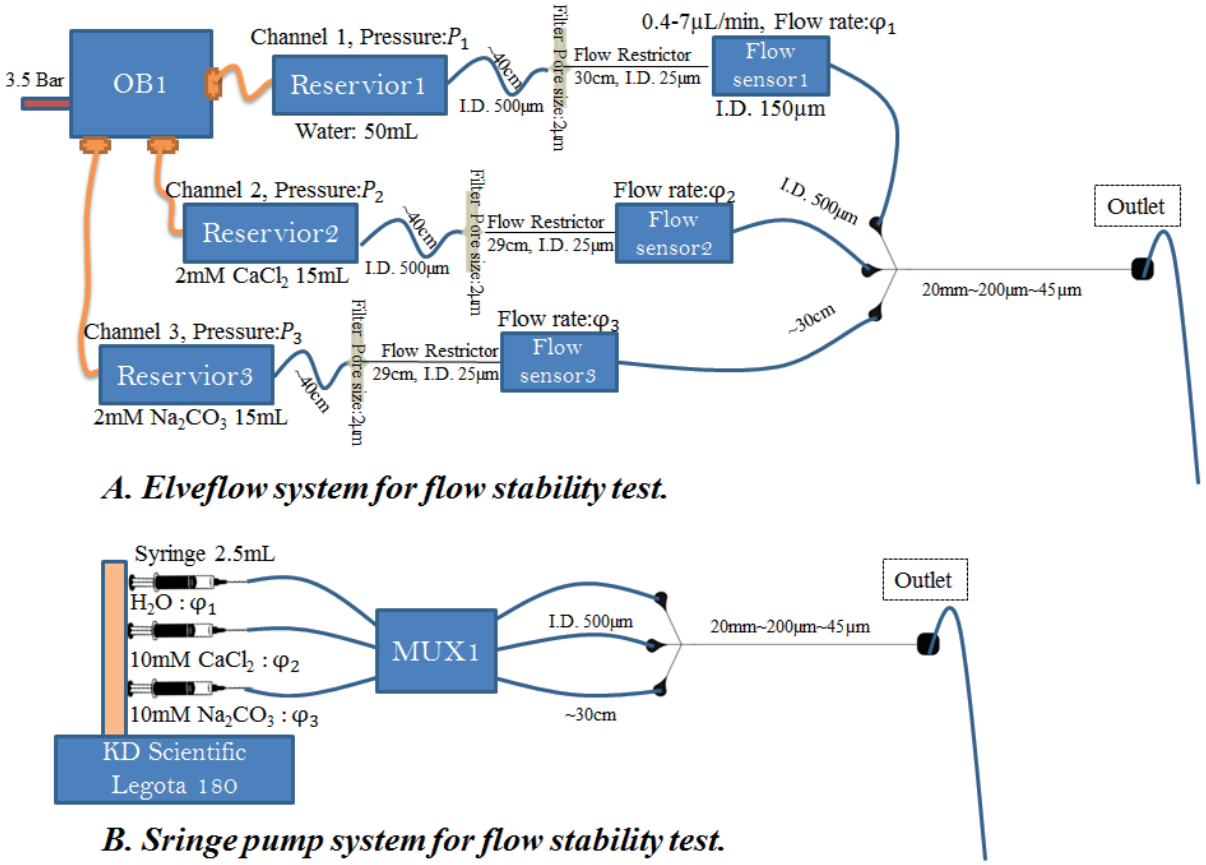

Figure 3.4: The setup of flow stability test. the upper shows the setup of OB1 pressure control flow system. The lower one shows the setup of syringe pump flow system.

at 1 μl/min and 1 input channel with dyed water at 2 μl/min and in four configurations: Gas pressure driven fluid flow with 1) pressure control (PC) and 2) flow control (FC) and syringe pump with 3) plastic syringe (PS) and 4) glass syringe (GS). The instantaneous volume fraction of dyed water presented in Figure 3.5 was calculated from images according to equation (3.2) and from the flow sensors. The data from the flow sensors and images shows that the OB1 control system is much better than the syringe pump system. Since the pressure in the channel increases all the time during the crystal growth. We decide to use the flow rate control model during the crystal growth experiments.

3.3 Calcite nucleation and growth

Before the nucleation in the microfluidic channel is started, Calcium chloride solution and sodium carbonate solution has to be prepared. Na_2CO_3 and $CaCl_2$ 10 mM stock solutions were prepared using a balance (Mettler AE260 Delta Range) and deionized water (Millipore Direct-Q 3UV) as solvent: 122.7 mg of Na_2CO_3 (VWR Ref.27767.364 Assay 99.0-100.5%) were dissolved in 115.6 mL water and 126.0 mg of $CaCl_2$Â·$2H_2O$ (VWR Ref.22322.364 Assay 97.0-103.0%) were dissolved in 85.7 mL water. Then, they were left to equilibrate with atmospheric CO_2 for 48 hours. Subsequently, 2 mM solutions were prepared by diluting the stock solutions with deionized water (2mL from

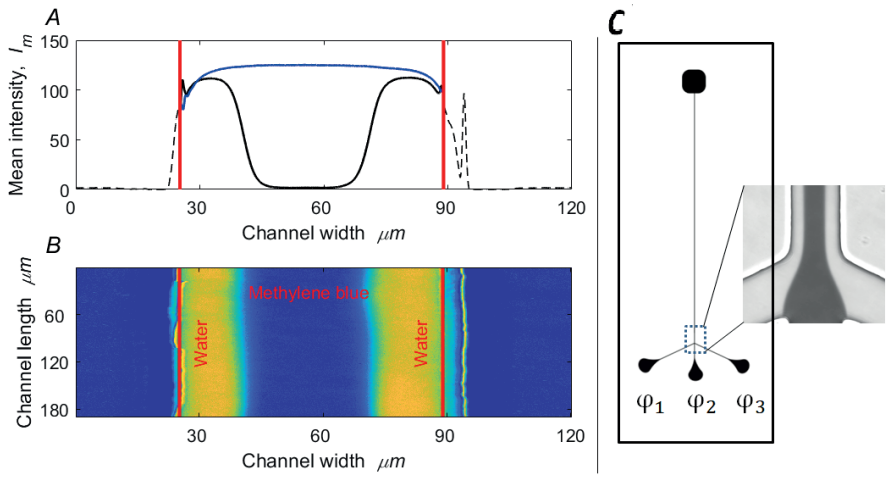

Figure 3.5: Calculation of the relative volume of water and methylene-blue from difference image. A: The mean intensities I_m along the width of the channel for water/methylene-blue/water solution (black line) and only water in the channel (blue line). The red vertical lines define the edge of the channel, x_1 and x_2. The black dashed line show the mean intensity outside the channel. B: The intensity difference between an image of water and methylene blue flowing in a part of the PDMS channel. C: The inset image shows the junctions where the colored and uncolored flows meet.

the stock solution were mixed with 8mL of deionized water) prior to each experiment. After dilution, they were immediately entered into pressure flasks using air at pressures between 1 and 2.2 atmospheres (absolute pressure). The saturation index, Σ has been calculated by PHREEQC [3]. The supersaturation is $\Omega = IAP/K_{sp}$ and the saturation index is

$$\Sigma = \frac{\Delta\mu}{kT} = \ln(\frac{a_{Ca^{2+}} a_{CO_3^{2-}}}{K_{sp}}) = \ln(\Omega) \tag{3.3}$$

We have used the value of the solubility product $K_{sp} = 10^{-8.54}$ that Teng et al. [24] found to correspond to when spirals on the $10\bar{1}4$ surface stopped growing. They used slightly different fluids than in our study and a fixed pH of 8.5, whereas our solutions were not buffered and the pH varied. The lack of constraints on pH causes some inaccuracy of the calculation of saturation index. In this study, the calcite crystals changed from growth to dissolution at a concentration of c_{sat}=0.5 mM. In order to nucleate and grow calcite in the microfluidic channel, we improved the microfluidic channel. Figure 3.7. The channel is 120±2 μm wide and 45 μm high, the length from first to second junction is l_c=50 mm and the length from the second junction to the outlet is 10 mm. Nucleation of a crystal within the microfluidic channel was carried out in two steps. First, the channel was filled with deionized water at a flow rate $\varphi_1 = 0.5\mu$l/min from inlet 2. 2mM $CaCl_2$ and Na_2CO_3 solutions were subsequently injected at inlets 1 and 3 to achieve a $CaCO_3$ concentration of c=0.8 mM. This value was sufficiently low to avoid any nucleation. When the flow reached a stable behavior, the 10mM $CaCl_2$ and Na_2CO_3 solutions, were injected into the channel from inlets 4 and 5 (using 2.5mL Halmiton 1000 syringes on a KD Scientific Legato 180 syringe pump) to achieve a $CaCO_3$ concentration of c =3.4 mM.

Once we observed crystals sticking to the glass or to the PDMS surface, the flows φ_4 and φ_5 were stopped. There is a certain probability that the first nucleus be either calcite, vaterite or aragonite, in our conditions the probability was roughly 50/50 cal-

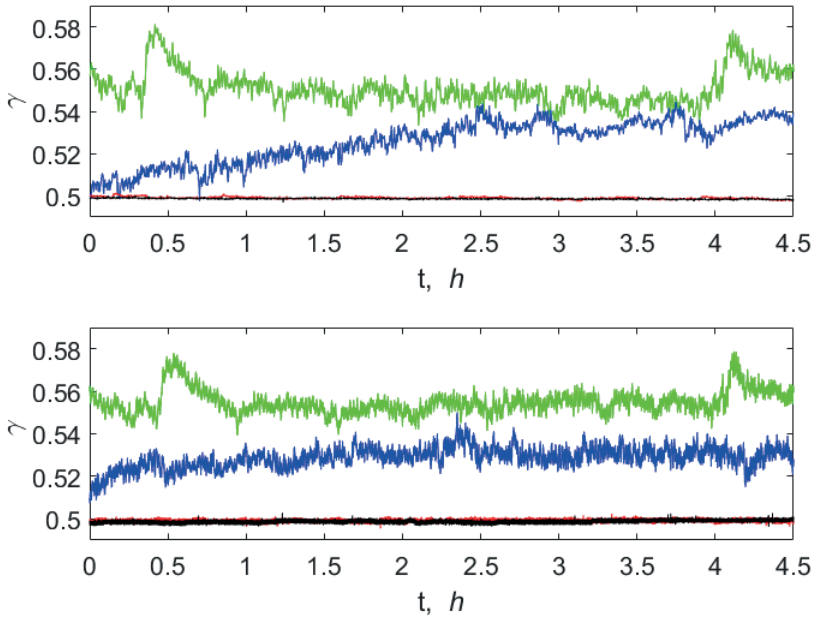

Figure 3.6: Stability of water/dyed water/water flow. The relative volume γ of dyed water calculated from images (top) and flow sensors (bottom) is displayed in black: pressure control (PC), red: flow control (FC), green: plastic syringe (PS) and blue: glass syringe (GS).

cite/vaterite in agreement with the measurements of Ogino et al [18]. In the remainder of the experiment we always chose to observe the crystal furthest upstream to be sure that the fluid concentration was determined by the flow rates and was not affected by other crystals upstream. Since the crystal is unaffected by other crystals and fully controlled by the concentration of the flowing solution we could dissolve and grow any $CaCO_3$ polymorph at will. Before calcite growth experiments we dissolved vaterite at $c = 0.5$ mM if present, while keeping the calcite crystal unchanged. We performed calcite growth rate experiments with concentrations in the range 0.55-0.8 mM.

At a saturation index of $c = 3.4$, nucleation occurs fast and some nuclei attach either to the PDMS or to the glass surfaces. Figure 3.9 A shows both a calcite and a vaterite nuclei present simultaneously in the middle of the channel. Since mixing occurs by diffusion, the highest concentration appears at the center of the channel and the nuclei are likely to attach close to the middle of the glass or PDMS surface allowing for good optical access and free space for subsequent growth. Changing the calcium carbonate concentration to 0.5 mM, the vaterite is totally dissolved after 22 minutes and the calcite is left unchanged (Figure 3.9 B). The calcite nuclei are predominantly rhombohedral and the $10\bar{1}4$ surface attach to the glass or PDMS. The crystals can then grow freely on 5 of the 6 surfaces. Figure 3.9 C shows a vaterite nucleus that is chosen for growth in the channel and Figure 3.9 D shows the same crystal after 23 hours growth. This demonstrates how the microfluidic device can keep any polymorph stable for further study.

After we succeed to nucleate and grow calcite in the microfluidic channel, we start the final step of our experiment: loading a force on the growing calcite. We put another channel on the top of the crystal growth channel. As shown in Figure 3.10, we could

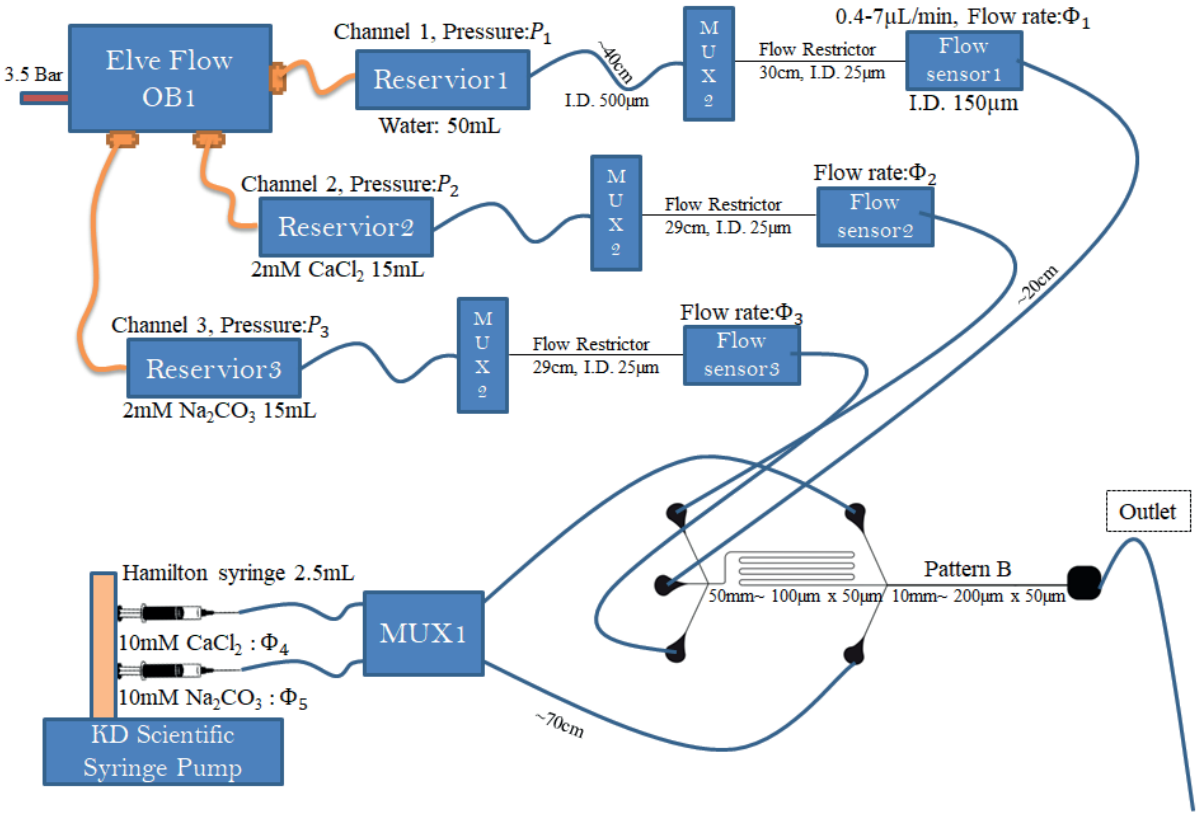

Figure 3.7: The experimental setup for calcite nucleation and growth.

calculate the pressure and force loaded on the growing calcite during its whole growth, by varying the pressure on the top channel (from 0 to 2 Bar).

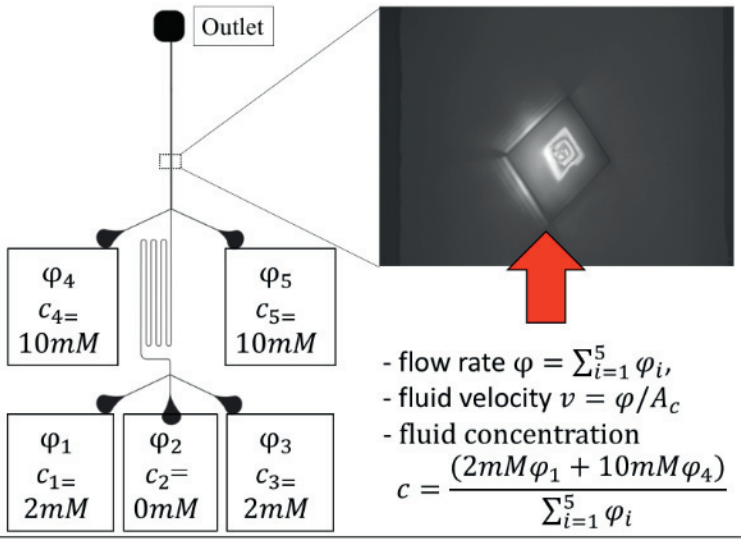

	φ_1 $\frac{\mu l}{min}$	φ_2 $\frac{\mu l}{min}$	φ_3 $\frac{\mu l}{min}$	φ_4 $\frac{\mu l}{min}$	φ_5 $\frac{\mu l}{min}$	φ $\frac{\mu l}{min}$	u $\frac{mm}{s}$	c mM
Nucl.	1	0.5	1	2	2	6.5	20	3.4
Growth	1	0.5	1	0	0	2.5	7.7	0.8
Sat.	1	2	1	0	0	4	12	0.5

Figure 3.8: Flow rate control for nucleation and growth. The fluid concentration in the channel at the crystal depends on the relative flow rates of the 5 inlets. $CaCl_2$ is injected through inlets 1 and 4 and Na_2CO_3 is injected through inlets 3 and 5. Inlets 4 and 5 are only used during nucleation to assure nucleation in the channel between the second junction and the outlet. During growth the concentration is varied by changing φ_2 in the range shown in the table.

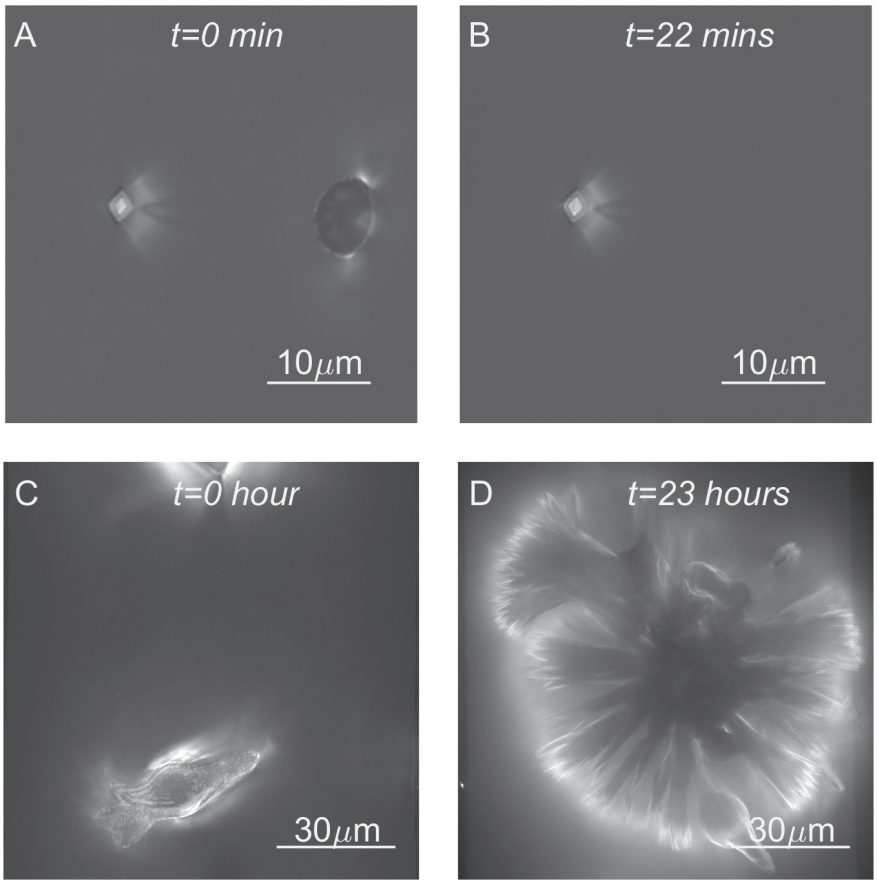

Figure 3.9: Top (A and B): A. Calcite and Vaterite nuclei at the same time and attached at the middle of the channel. B. The vaterite disappeared after 22 minutes flushing with 0.5mM $CaCO_3$ solution. Bottom C.D: C. A aragonite located in the channel. D. The aragonite grows to fill the channel after 7 hours growth at 0.8 mM $CaCO_3$ concentration. The radius of aragonite crystal increase at a rate of 4160 nm/h.

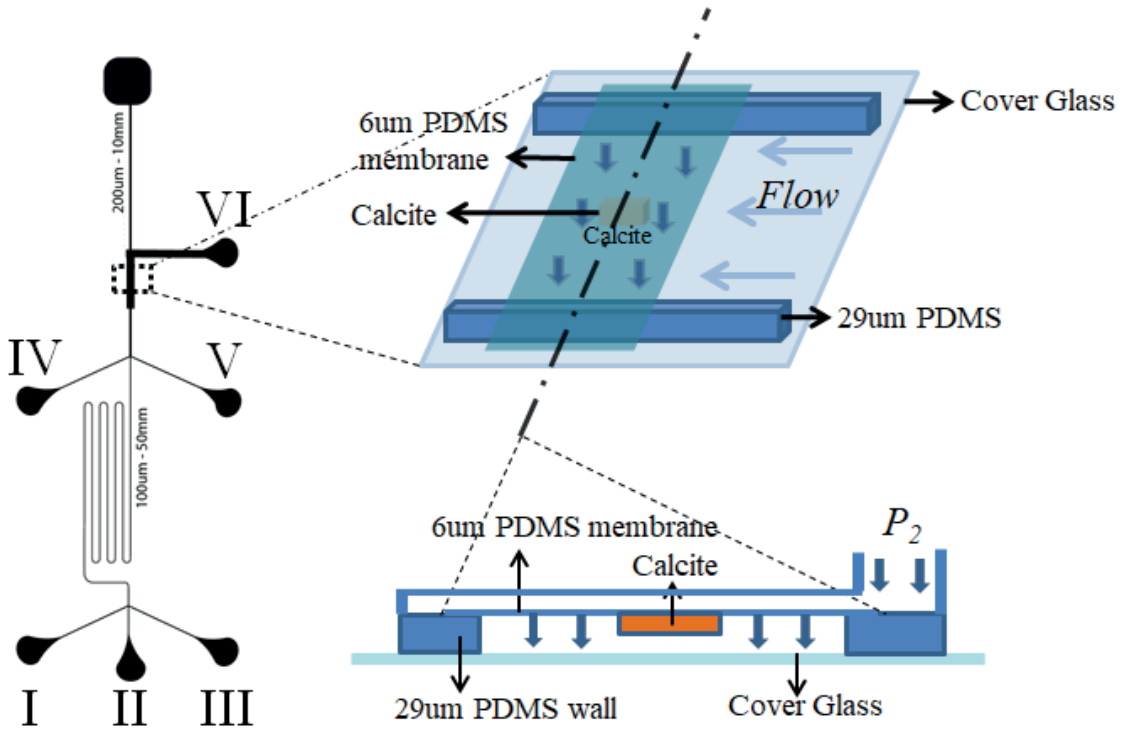

Figure 3.10: In this new microfluidic chip, we put another channel on the top of the crystal growth channel. By controlling the pressure in top channel, we could control the loaded force on the crystal. The pressure varies from 0 to 2 Bar.

CHAPTER 4

Results and Outlook

In this work, we succeed to nucleate and grow calcite in a 45μm wide microfluidic channel. Also, we control the pressure on the growing calcite. Since the Reynolds number in the channel is less than 1, there is definitely no turbulence or convection in the channel. We controlled the boundary condition of the growing crystal since we have a good control of the fluid flow rate in the channel. Of course, the whole experiment is get rid of the dust, even without bacterium. By varying the $CaCO_3$ concentration, we could keep the calcite and remove the vaterite and aragonite in the channel.

In paper I, we demonstrate how to nucleate and grow calcite in the channel. We also demonstrate that at low supersaturations where 2D nucleation does not occur we measure the growth rate constant of calcite to be a factor 5 larger than that reported by batch methods and a factor 50 larger than measured by AFM. The growth rate difference is due to the difference of the hydrodynamic boundary layer. According to our calculation, the AFM experiment's boundary layer is 10-50 times thicker than our experiment. And also, the boundary layer difference well explains the different growth rates on the front and back side of the crystal.

In paper II, we present a novel approach to in situ study of confined crystal growth using microfluidics for accurate control of the saturation state of the fluid and interferometric measurement of the topography of the growing confined crystal surface. We observe and quantify diffusion limited confined growth rims and explain them with a mass balance model. We have quantified and modeled crystals "floating" on a fluid film of 25-50 nm thickness due to the disjoining pressure. We find that there are two types of nanoconfined growth behaviors: 1) smooth and 2) rough intermittent growth, the latter being faster than the former. The intermittent growth rims have regions of load bearing contacts that move around the rim causing the crystal to "wobble" its way upwards. A first step to understand the intermittent dynamics is the identification of a local, positive feedback between load and growth rate.

In paper III, a 2-layer microfluidic chip is used in the experiment, which allows force actuation on growing calcite. When we press a flat calcite surface towards a cover glass, the calcite surface gets confined immediately and forms a cavity on the confined surface, even if the pressure is quite low. After we increase the pressure, vertical growth of the calcite slows down dramatically (due to the shrinkage of the confined fluid film and the decrease of diffusion constant). And also the rim width increase during the growth. We carefully analyzed the relationship between loaded pressure, film thickness, the rim

width and calcite vertical growth rate by the mass balance and force balance, which help us to understand the crystal growth under confinement.

I believe that the experiment could be improved in the future. The pressure system could be more accurate. For example, the pressure could vary from DLVO pressure to hydration force and the the theoretical crystallization pressure. I hope the crystal could dissolve when the pressure exceed the theoretical crystallization pressure. The resolution of RICM is not good enough when the confined film is less than 100 nm. The deviation of thickness measurement in this paper is 10nm. From the paper 2, we could find that the calcite grows really beautyful when it is confined by its own weight. The crystal surface is parallel to cover glass. But when we try to load a force on the crystal, it is extremly difficult to keep the crystal surface parallel to the cover glass. It is very challenging to measure the contact area. It would be interesting to see the crystal grows with different loaded forces. It will help people a lot to understand the crystal growth.

At the end of my thesis, I want to leave some words to myself. To finish my Ph.D degree in Europe is my dream. Now, it is going to be true. Why did the science and industrial revolution happen in Europe? That was the question haunting in my mind all the time. Now I get the answer, it is the serious attitude to science. Being a Ph.D is just like walking through a long dark mysterious tunnel. Unfortunately, there is no candle or LED light. Several years ago, when I stood in front of the tunnel, I was so excited. My supervisor Dag told me that it is so much fun in the tunnel. Then I stepped into the tunnel. As I walked deeper and deeper, I found myself lost. It is eventually dark. So many times, when I lost my way in the tunnel, Dag scratched a match in front. The shaking light of match seems like the tunnel exit. It encouraged me to go further. More than once, I have complained. Why can't the match light longer? Now I could see the tunnel. It is full of burnt matches, and they have burnt to the last inch. Thanks to Dag, I respect your attitude to science. And also you are so kind of taking care of us Ph.D students. Thanks to Anja and Felix, without your help, I can't be here. I will never forget the time in UiO. Thank you!

Bibliography

[1] G. F. Becker and A. L. Day. The linear force of growing crystals. 7:283–288, 1905.

[2] C.-F. Chang and J.-W. Chen. The experimental investigation of concrete carbonation depth. *Cement and Concrete Research*, 36(9):1760–1767, 2006.

[3] S. R. Charlton and D. L. Parkhurst. Modules based on the geochemical model phreeqc for use in scripting and programming languages. *Computers & Geosciences*, 37(10):1653–1663, 2011.

[4] C. W. Correns. Growth and dissolution of crystals under linear pressure. *Discussions of the Faraday society*, 5:267–271, 1949.

[5] B. Deraguin and L. Landau. Theory of the stability of strongly charged lyophobic sols and of the adhesion of strongly charged particles in solution of electrolytes. *Acta Physicochim: USSR*, 14:633–662, 1941.

[6] J. Desarnaud, O. Grauby, P. Bromblet, J.-M. Vallet, and A. Baronnet. Growth and dissolution of crystal under load: new experimental results on kcl. *Crystal Growth & Design*, 13(3):1067–1074, 2013.

[7] J. Desarnaud, D. Bonn, and N. Shahidzadeh. The pressure induced by salt crystallization in confinement. *Scientific reports*, 6:30856, 2016.

[8] Y. Diao and R. M. Espinosa-Marzal. Molecular insight into the nanoconfined calcite–solution interface. *Proceedings of the National Academy of Sciences*, 113 (43):12047–12052, 2016.

[9] R. J. Flatt, M. Steiger, and G. W. Scherer. A commented translation of the paper by cw correns and w. steinborn on crystallization pressure. *Environmental geology*, 52(2):187, 2007.

[10] R. J. Flatt, F. Caruso, A. M. A. Sanchez, and G. W. Scherer. Chemo-mechanics of salt damage in stone. *Nature communications*, 5:4823, 2014.

[11] J.-P. Gratier, E. Frery, P. Deschamps, A. Royne, F. Renard, D. Dysthe, N. Ellouz-Zimmerman, and B. Hamelin. How travertine veins grow from top to bottom and lift the rocks above them: The effect of crystallization force. *Geology*, 40(11): 1015–1018, 2012.

[12] J.-P. Gratier, D. K. Dysthe, and F. Renard. The role of pressure solution creep in the ductility of the earths upper crust. 54:47–179, 2013.

[13] J. N. Israelachvili. Intermolecular and surface forces. 2011.

[14] J. N. Israelachvili and G. E. Adams. Measurement of forces between two mica surfaces in aqueous electrolyte solutions in the range 0–100 nm. *Journal of the Chemical Society, Faraday Transactions 1: Physical Chemistry in Condensed Phases*, 74:975–1001, 1978.

[15] J. Lavalle. Recherches sur la formation lente des cristaux à la température ordinaire. *Compte Rend. Acad. Sci.(Paris)*, 36:493–495, 1853.

[16] S. M. Mutisya, A. Kirch, J. M. De Almeida, V. M. Sanchez, and C. R. Miranda. Molecular dynamics simulations of water confined in calcite slit pores: an nmr spin relaxation and hydrogen bond analysis. *The Journal of Physical Chemistry C*, 121(12):6674–6684, 2017.

[17] A. Naillon, P. Joseph, and M. Prat. Ion transport and precipitation kinetics as key aspects of stress generation on pore walls induced by salt crystallization. *Physical review letters*, 120(3):034502, 2018.

[18] T. Ogino, T. Suzuki, and K. Sawada. The formation and transformation mechanism of calcium carbonate in water. *Geochimica et Cosmochimica Acta*, 51(10): 2757–2767, 1987.

[19] J. Ploem. Reflection-contrast microscopy as a tool for investigation of the attachment of living cells to a glass surface. 1975.

[20] E. Rothrock. On the force of crystallization of calcite. *The Journal of Geology*, 33 (1):80–83, 1925.

[21] K. Sekine, A. Okamoto, and K. Hayashi. In situ observation of the crystallization pressure induced by halite crystal growth in a microfluidic channel. *American Mineralogist*, 96(7):1012–1019, 2011.

[22] P. T. Staudigel and P. K. Swart. Isotopic behavior during the aragonite-calcite transition: Implications for sample preparation and proxy interpretation. *Chemical Geology*, 442:130–138, 2016.

[23] S. Taber. The growth of crystals under external pressure. *American Journal of Science*, (246):532–556, 1916.

[24] H. H. Teng, P. M. Dove, and J. J. De Yoreo. Kinetics of calcite growth: surface processes and relationships to macroscopic rate laws. *Geochimica et Cosmochimica Acta*, 64(13):2255–2266, 2000.

[25] E. J. W. Verwey, J. T. G. Overbeek, and J. T. G. Overbeek. Theory of the stability of lyophobic colloids. 1999.

[26] B. H. Wilkinson. Biomineralization, paleoceanography, and the evolution of calcareous marine organisms. *Geology*, 7(11):524–527, 1979.

[27] S. Yoshioka and Y. Kitano. Transformation of aragonite to calcite through heating. *Geochemical Journal*, 19(4):245–249, 1985.

PUBLICATION 2

Growth of Calcite in Confinement

Lei Li, Felix Kohler, Anja Røyne and Dag Kristian Dysthe. *Crystals*, **316**, 7 (2017).
https://www.mdpi.com/2073-4352/7/12/361

crystals

MDPI

Article

Growth of Calcite in Confinement

Lei Li, Felix Kohler, Anja Røyne and Dag Kristian Dysthe *

Condensed Matter Section and Physics of Geological Processes, Department of Physics, University of Oslo, P. O. Box 1048 Blindern, 0316 Oslo, Norway; lei.li@fys.uio.no (L.L.); felix.kohler@fys.uio.no (F.K.); anja.royne@fys.uio.no (A.R.)

* Correspondence: d.k.dysthe@fys.uio.no; Tel.: +47-9094-0996

Academic Editor: Hugo K. Christenson

Received: 7 July 2017 ; Accepted: 30 November 2017; Published: 6 December 2017

Abstract: Slow growth of calcite in confinement is abundant in Nature and man-made materials. There is ample evidence that such confined growth may create forces that fracture solids. The thermodynamic limits are well known, but since confined crystal growth is transport limited and difficult to control in experiments, we have almost no information on the mechanisms or limits of these processes. We present a novel approach to the in situ study of confined crystal growth using microfluidics for accurate control of the saturation state of the fluid and interferometric measurement of the topography of the growing confined crystal surface. We observe and quantify diffusion-limited confined growth rims and explain them with a mass balance model. We have quantified and modeled crystals "floating" on a fluid film of 25–50 nm in thickness due to the disjoining pressure. We find that there are two end-member nanoconfined growth behaviors: (1) smooth and (2) rough intermittent growth, the latter being faster than the former. The intermittent growth rims have regions of load- bearing contacts that move around the rim causing the crystal to "wobble" its way upwards. We present strong evidence that the transition from smooth to rough is a generic confinement-induced instability not limited to calcite.

Keywords: crystal growth; calcite; microfluidic; nanoconfinement; reflection interference contrast microscopy

1. Introduction

A number of marine organisms mineralize calcium carbonate [1]. The biomineralization processes are of great interest in themselves, and confinement in cellular compartments is thought to be important in the process of controlling biological mineral growth [2]. The organisms with calcium carbonate skeletons sediment to the sea floor, and the sediments undergo compaction where dissolution and recrystallization of calcite occur in confinement to form limestone [3]. Some such carbonate rocks are buried deeper and undergo recrystallization in confinement once more and emerge as marble. Both limestone and marble are used for construction and sculptures that deteriorate due to confined salt crystallization in the pore space [4]. In Portland cement, CO_2 is slowly adsorbed, and calcite is crystallized in confinement [5]. Confined recrystallization of calcite in other environments has also been shown to create forces that break other mineral grains [6] and lift rock overburden [7].

The above examples show that carbonate rocks, where the pore fluid becomes supersaturated in calcium carbonate, behave in two completely different manners: sometimes, the calcite crystallizes in the pore space and around grain contacts and cements and strengthens the rock [3], and sometimes, calcite crystallizes in the grain contacts and breaks the surrounding rock [6,7]. Except for a general equilibrium thermodynamic argument for the limit to the force of crystallization [8–10], there exists no experimental data or theoretical models to understand the transition from crystallization force to cementation [11]. The general question "when does crystallization in confinement lead to stress

buildup and damage, and when does crystallization cease due to confinement?" is also central to understanding salt damage of building materials like limestone and concrete and monuments [4,12,13]. Knowledge about the limits to crystallization pressure is also at the core of the ongoing debate on the effects of stress on metamorphism in the Earth's crust [14,15].

There are three main types of experiments that have been performed to study the stresses generated by crystallization: high temperature, high pressure experiments with mineral transformations where the degree of growth of secondary minerals is studied ex situ [15], salt crystallization in porous rocks where dilation, damage and fracturing is studied [13] and, finally, studies on single crystals growing against a known force [9,11,16,17]. Only a limited number of successful such experiments have been performed since Becker and Day studied potassium alum [16]. Becker and Day [16] documented that the contact area between the growing crystal and the support was much smaller than the apparent surface area and went to great lengths to determine this area because the force on the crystal divided by the contact area equals the contact pressure, which is the relevant thermodynamic variable. Taber [17] studied potassium alum, chrome alum, potassium sulphate and copper sulphate and found that the existence of other crystals in the crystallization chamber stopped the crystallization doing work against an external force. Correns performed a series of experiments on potassium alum, sodium carbonate and calcium chloride published between 1926 and 1949 culminating in a seminal paper with data on the maximum pressure at which there is crystallization doing work and provided a thermodynamic expression for the relation between stress and supersaturation [9]. Curiously, the thermodynamic expression has an excellent fit with the experimental data, but is wrong by a factor of four [18], and despite his knowledge of the work of Becker and Day, he does not comment on the area of contact between the crystal and the glass support. The first carefully-controlled single-crystal crystallization pressure experiment since Correns was performed by Røyne and Dysthe on sodium chlorate [11,19].

Whereas the transport of material to a nanoconfined growth surface from melt (for instance, ice or metals) is dominated by viscous flow, transport during growth from solution is dominated by diffusion through the solution to the growing surface. If there is some force pressing the growing crystal against an impermeable solid, there may still be a confined fluid film between the two solid surfaces supporting the load, as long as the applied contact pressure does not exceed the maximum disjoining pressure [20,21].

The rate of crystal growth increases with supersaturation, and supersaturation decreases in the direction of diffusion (that is, driven by a concentration gradient). Therefore, there will be a negative feedback between growth and transport in the confined fluid. If the fluid supports sufficient stress, continuum theory predicts a smooth growth rim of well-defined, pressure-dependent width to appear at the confined growing surface [10]. Experiments documenting such growth rims during crystal growth confined by a glass plate and creating a force have been performed on potassium alum [16] and $NaClO_3$ [11]. These experiments show, however, that the confined growth surface is much more complex than the smooth rims predicted by continuum theory: the rims are rough, and their width does not depend on the load on the crystal in a systematic manner. This signifies that there are other, positive feedback mechanisms at work.

The present study of the growth of single crystals of calcite targets some of the many open questions from these earlier studies [9–11,16]: What is the area of contact between a crystal lifting a load and the base that it rests on? What are the characteristics of the interface topography? What is the contact stress? What are the processes controlling the interface topography and the contact area? Are these processes independent of solubility and growth rate?

Here, we report confined crystal growth experiments that differ from previous experiments in two respects: (1) instead of highly soluble crystals, we use calcite, which has a solubility of about four orders of magnitude smaller, and the growth rate is 3–4 orders smaller than $NaClO_3$; (2) we study the evolution of the growing confined crystal surface in situ. We measure the distance from

the confining surface to the crystal surface while it evolves and can thereby demonstrate positive and negative transport-growth feedback mechanisms due to nanoconfinement.

2. Experimental Section

The experiments reported here are designed to have a very high degree of control of the growth conditions and high resolution measurement of the topography of the confined crystal surface while it grows.

2.1. Microfluidic Growth Control

The microfluidic network and flow control system, which has been described in detail in [22], is designed to:

- nucleate calcium carbonate crystals in a limited area that permits imaging access;
- remove other polymorphs than calcite (polymorphs are determined by the crystal shape);
- control stable saturation conditions at the growing crystal surface;
- permit slow growth of rhombohedral crystals from the nuclei;
- avoid clogging of the microfluidic device due to crystal growth elsewhere in the device.

The main idea of the experiment is sketched in Figure 1. $CaCl_2$ solution and Na_2CO_3 solution at equal concentrations and flow rates are introduced in two inlets, and in the third inlet, distilled water is introduced to control the total concentration c of $CaCO_3$ in the main channel. The growth rate of the crystal (green in Figure 1) depends on the supersaturation $\Omega = (c - c_0)/c_0$, where c_0 is the equilibrium concentration, which is measured in situ as the concentration where the crystal neither grows nor dissolves, $c_0 = 0.50 \pm 0.02$ mM.

The channel networks are designed in Adobe Illustrator, saved as pdfs, and the photomask was printed on film substrate by Selba S.A (www.selba.ch). SU-8 GM1070 photoresist from Gersteltec (Pully, Switzerland) was spun on silicon wafers, UV radiated with UV-KUB2 (Montpellier, France) and developed with PGMEA from Sigma Aldrich (CAS no. 108-65-6, Darmstadt, Germany) according to the producer's data sheet. Channel networks were cast in PDMS (Sylgard 184 elastomer kit purchased through VWR, Brooklyn, NY, USA) in a 1:10 ratio of elastomer to curing agent, with 1.5 mm-diameter holes punched for inlets and outlets, and the PDMS and glass (VWR collection 24 mm × 24 mm cover glass No. 1) were plasma treated (Zepto BD-20V, from Diener Electronic GMBH, Bielefeld, Germany) before assembly. Flow rate was controlled using a syringe pump (Legato 180 from Kd Scientific, Holliston, MA, USA) with glass syringes (Halmiton 1000 syringe series, Bonaduz, Switzerland) and a fluid flow control system (OB1 mk3 from Elveflow, Paris, France). The channels most used in this study were 120 μm wide and 45 μm high; the distance from the inlet to the imaging site was 10–50 mm; and flow rates during growth in the range 0.2–1 μL/min.

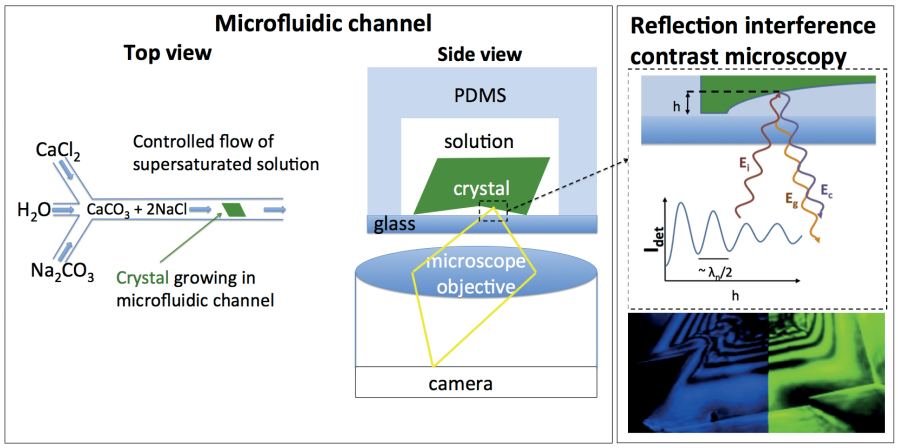

Figure 1. Controlled growth of calcite crystals in a microfluidic device studied by reflection interference contrast microscopy (RICM). (**Left**) Top view of the microfluidic channel showing how fluids are introduced and mixed to ensure stable supersaturation at the crystal surfaces. The microfluidic device rests on an inverted microscope to allow high resolution imaging of the crystal in situ during growth. The crystal grows on all surfaces, but the surface studied here is confined by the glass surface on which the crystal rests. (**Right**) Principle of RICM. The crystal is illuminated from the bottom, which is illustrated here by the electric field, E_i, of the incident light. Due to the interference of the light reflected by the crystal-water interface, E_c, with the light reflected by the glass-water interface, E_g, the detected intensity, I_{det}, depends on the distance, h, between the two interfaces and on the wavelength of the light, λ. Exemplary RICM images of a calcite crystal using a blue LED (left half) and a green LED (right half) are shown at the bottom. The fringes align at the outer part (rim) of the crystal, but differ for larger distances h towards the central part of the confined interface.

2.2. Topography Measurements

The crystal growth on the confined interface facing the glass is measured by reflection interference contrast microscopy (RICM). The basic principle of RICM is illustrated in Figure 1. The incident LED light from the microscope is reflected both from the crystal-water interface and from the glass-water interface. Thus, a part:

$$I_r \propto E_g^2 + E_c^2 + E_g E_c \cos(4\pi hn/\lambda + \pi) \quad (1)$$

of the total intensity $I_{det} = I_0 + I_r$ reaching the detector is given by the interference of these two reflected parts of the incident light, where E_g is the electromagnetic wave amplitude of the light reflected at the glass-water interface, E_c is the electromagnetic wave amplitude of the light reflected at the crystal-water interface, λ is the wavelength of the light, h is the distance between the glass and the crystal and $n = 1.33$ is the refractive index of water. I_0 denotes the part of the light reaching the detector by scattering at other interfaces of the system. Here, the light is represented by its central beam. The effects of the finite aperture of the imaging systems are not considered.

The reflected interference contrast can be achieved with almost any microscope using reflected light illumination. The contrast (I_r/I_0) can be augmented by using specialized objectives with a $\lambda/4$ retarder [23], but in this study, we have used ordinary objectives (UPLanFLN 100×/1.30 and UPLanFI 40×/0.75 from Olympus www.olympus-lifescience.com) mounted on an Olympus GX71 inverted microscope with a green LED light source with a wavelength of 550 nm (from ThorLabs www.thorlabs.com). Images are recorded with a monochromatic CCD camera with 3376 × 2704 resolution (Grasshopper3, GS3-U3-91S6M-C from Pointgrey www.ptgrey.com) and saved as 8-bit TIFF files. The image sequences are analyzed by in-house-developed scripts in MATLAB (www.mathworks.com) and ImageJ (imagej.nih.gov/ij/).

3. Results

We present in situ images of how the crystal surfaces confined by the glass surface evolve during stable growth conditions. We quantify and summarize the common behavior and display the variations in growth habit that may help us and the reader to interpret the reasons for the variability in quantifiable parameters. To our knowledge, no one has observed such confined crystal growth in situ before, and we therefore also document and quantify behavior that we cannot explain in detail. We focus on two crystals, but more examples of other crystals are documented in the Supplementary Materials, Figures S1–S5 and to videos, CrystalA.avi and CrystalB.avi.

3.1. Interpretation and Quantification of In Situ Image Data

The series of images in Figure 2A shows the growth outwards and upwards of Crystal A at $c = 0.8$ mM ($\Omega = 0.6$). Dark areas along the rim of the crystal signify areas of contact between the crystal and the glass. The distance h between the crystal and the glass in the contact region varies in the range $h = 40$–50 nm. The area outside the crystal is much brighter on the left and upper side of the crystal than on the lower and right side due to reflections from the different sides of the rhombohedral crystal. This difference in intensity can be used to determine the orientation of the crystal.

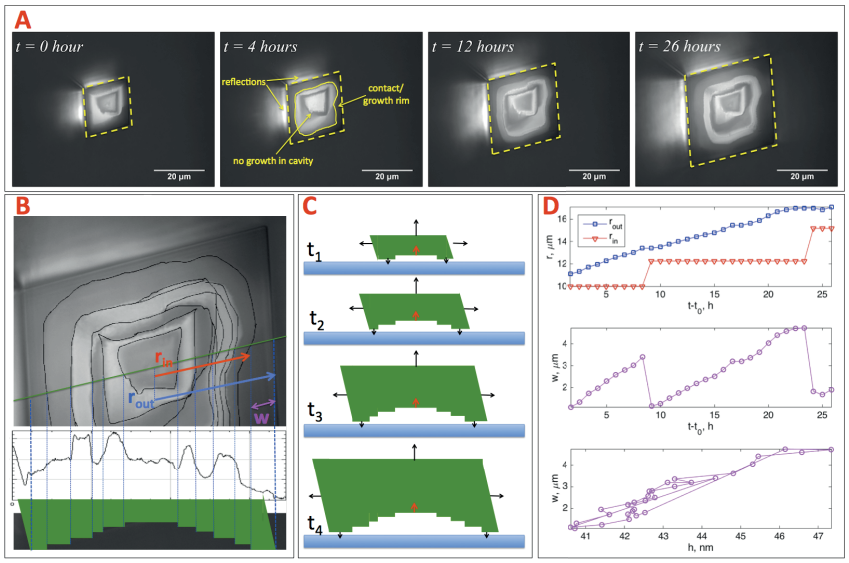

Figure 2. In situ imaging of 26 h of growth of Crystal A, raw data and interpretations: $\Omega = 0.6$, flow direction bottom to top. (**A**) In situ images of the growing $10\bar{1}4$ calcite crystal surface confined by glass, imaged from below (see Figure 1). For a full time-lapse movie of the same crystal, see the movie CrystalA.avi. The crystal outline is marked by a dashed line. Dark areas along the rim of the crystal (between the dashed line and whole drawn line in the image at 4 h) signify areas of contact between crystal and glass. The bright, diffuse areas to the left and above the crystal are reflections from the two rhombohedral crystal sides that "overhang" the contact. The time $t = 0$ is an arbitrary reference time. (**B**) Top: Lines of the inner rim edge position of Crystal A at different times are drawn on the final crystal surface. Middle: Intensity in the image along the green line. Bottom: A sketch of a cut through the crystal along the green line showing the profile of the confined crystal surface. Vertical lines are drawn connecting the image, the intensity plot and the interpreted profile. (**C**) Interpretation of the image sequence in (A). The crystal grows (black arrows) freely on the top and outer surfaces, as well as on the lower surface confined by the glass, causing the crystal to be lifted upwards (red arrow). There is no growth of the crystal in the cavity that forms inside the rim; (**D**) Top: Inner, r_{in}, and outer, r_{out}, radius the of crystal as a function of time. Middle: Rim width, $w = r_{out} - r_{in}$, versus time. Bottom: Rim width versus distance to glass surface, h.

Figure 2B shows Crystal A after 26 h with all the former inner boundaries of contact rims drawn in. In the video CrystalA.avi, we drew a line every time the outer rim contact developed a new rim with lower intensity. We observe that the topography of steps at the confined crystal surface are relics of dynamic changes in step flow growth.

The plot of the inner, r_{in}, and outer, r_{out}, radius of the crystal as a function of time in Figure 2D (top) shows that the outer surfaces of the crystal grow at a constant rate (310 ± 9 nm/h), while the inner radius of the growth rim, r_{in} (radius of cavity), moves stepwise. The rim width versus time shown in Figure 2D (middle) therefore repeatedly grows to a maximum of 4–5 µm and suddenly jumps to a minimum of 1–2 µm. The distance between the crystal growth rim and the glass, h, calculated using Equation (1) is found to increase linearly with rim width, w (Figure 2D, bottom) [24].

Assuming equal growth rate on the top and outer surfaces of the crystal, the distance r from the center of the bottom surface to the outer sides and to the top are approximately equal. The volume of the crystal is therefore approximately $V = 4r^3$. The weight of the crystal resting on the contact areas of the growth rim is therefore $F = V(\rho_c - \rho_s)g$, where the crystal density is $\rho_c = 2700$ kg/m^3 and the solution density is $\rho_s = 1000$ kg/m^3. During the 26 h shown in Figure 2, r grows linearly in time from 9–17 µm, and the rim width w fluctuates between approximately one and five micrometers. The contact area is $A_c = 8wr$, and the average pressure at the contact surface is $P = F/A_c = r^2(\rho_c - \rho_s)g/(2w)$, ranging between 0.14 and 2.42 Pa.

Figure 3 shows in situ images of the confined $10\bar{1}4$ surface of Crystal B at $c = 0.7$ mM ($\Omega = 0.4$) with a contact rim evolution that is very distinct from Crystal A. Crystals A and B may be considered representatives of two different families of behavior that we have observed in 20–30 crystal growth experiments: smooth rim growth and intermittent rim growth, both with rims actively lifting the crystal. Both rough and smooth rim evolutions occur in the same range of supersaturations $\Omega \in \{0.4\text{–}0.6\}$.

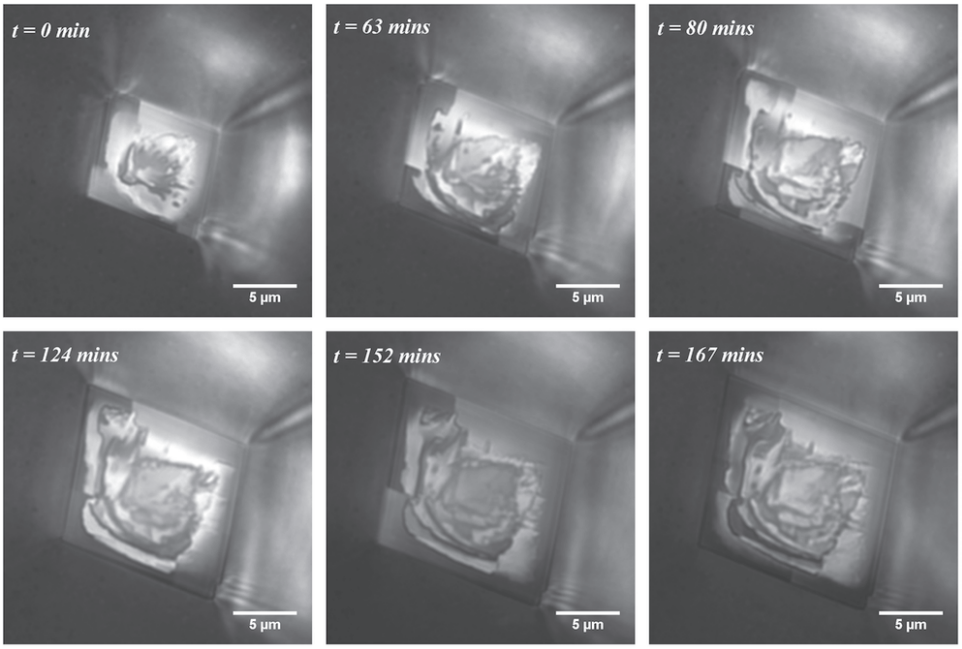

Figure 3. *Cont.*

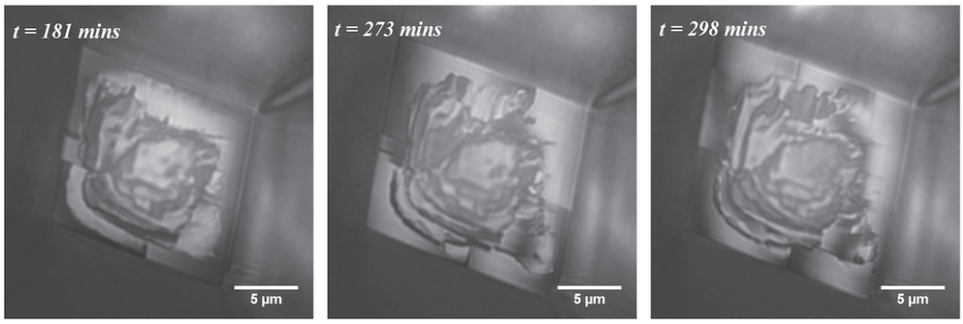

Figure 3. Six hours of growth of Crystal B at $\Omega = 0.4$. Dark areas along the rim of the crystal signify areas of contact between crystal and glass. One observes that for Crystal B, these contact areas move intermittently from place to place along the rim with time.

In the image sequences of all crystals (here and in the Supplementary Material), one may observe that crystal surface topography inside the "cavity" is conserved. The fact that the crystal surface inside the cavity does not change indicates that the solution inside the cavity must be at equilibrium with the crystal surface. We can therefore use the vertical motion of the crystal surface inside the cavity (red arrow in Figure 2C) as a measure of the growth rate at the confined crystal surface. In this analysis, we neglect the 10 nm up and down change in crystal-glass distance shown in Figure 2D. We can therefore measure the growth rate $v = dh/dt$ of the crystal at the rim by measuring the change of intensity $I(t)$ inside the cavity with time. Figure 4 shows intensity data $I(t)$ from the middle of Crystal B's (see Figure 3) surface with time. The minima (blue squares) and maxima (red squares) are used to rescale all intensity data points in between the range $[-1, 1]$: $\hat{I}(t)$. Using an approximation for low numerical aperture objectives, the distance h between crystal and glass is:

$$h(t) - h(t_0) = \frac{\lambda}{4n}\left(2m + \pi \arcsin\left(\hat{I} + \phi\right)\right) \tag{2}$$

where m is an integer counting the number of periods and ϕ the phase shift corresponding to the distance $h(t_0)$. The right-hand panel of Figure 4 shows the change in height, $h(t) - h(t_0)$, calculated using the intensity data shown in the left-hand panel. The least squares fit yields the vertical growth rate $v = dh/dt$ with the standard deviation. This value of v is used with a smooth amplitude function to produce the fit (red dashed line) to the original data in the left panel of Figure 4.

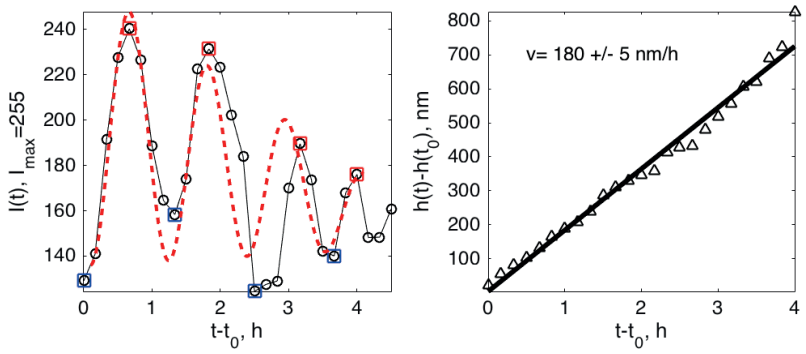

Figure 4. (**Left**) Intensity in the middle of Crystal B's (see Figure 3) surface with time. Circles denote data from images; blue and red squares are data points used to rescale the amplitude before applying arcsine. The red dashed line shows the fit to data. (**Right**) Triangles' height is calculated from intensity data as a function of time, and the black line is the least squares fit.

While Crystal A displays a stable, smooth growth rim, confining a fluid film with a uniform thickness of 40–50 nm, the growth rim of Crystal B is rough, with contact areas that move about on the crystal rim and fluid film thicknesses that vary in space and time. The dynamics is illustrated in Figure 5. This complex dynamics of moving contact points and large fluid film thicknesses causes the crystal to tilt and wobble.

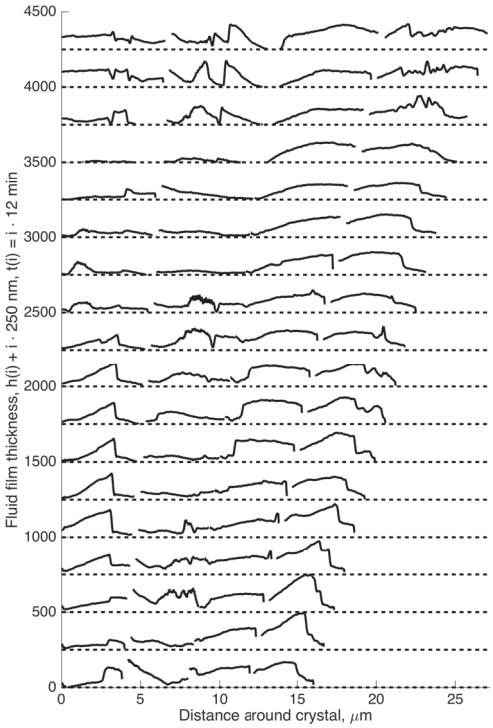

Figure 5. Profiles of the crystal: glass distance (fluid film thickness), h, around the rim of Crystal B at different times. Each new profile is shifted 250 nm up to separate them.

The distribution of fluid film thicknesses along the outer crystal rim during 4 h of growth is shown in Figure 6. This distribution shows one peak around 25 nm and another around 90 nm. We consider these height values to have no more than 20% accuracy due to the difficulty of calibrating the height for varying background light conditions at the different edges. The two distinct peaks of the fluid film thickness distribution are robust.

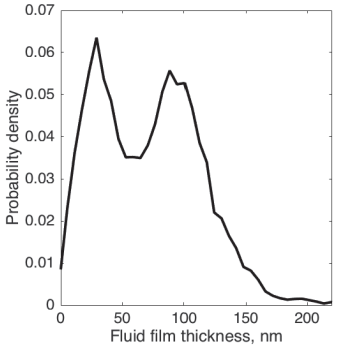

Figure 6. Probability distribution of fluid film thicknesses along the rim of Crystal B.

All crystals we have observed have either smooth or rough growth rims. Figure 7 shows that a smooth growth rim can become unstable and roughen. We have only observed this transition from smooth to rough, not from rough to smooth. Thus, in the concentration (supersaturation) interval [0.7, 0.8] ([0.4, 0.6]), both smooth and rough growth rims occur. Rough surfaces change dynamically, "mountains" and "valleys" appearing and disappearing with time. Smooth surfaces may be destabilized to roughen, but this has been observed only for small (<10 μm) crystals; larger smooth crystals stay smooth. Thus, the available evidence suggests that below a certain size, a growing crystal may evolve into one of two states, and that state persists.

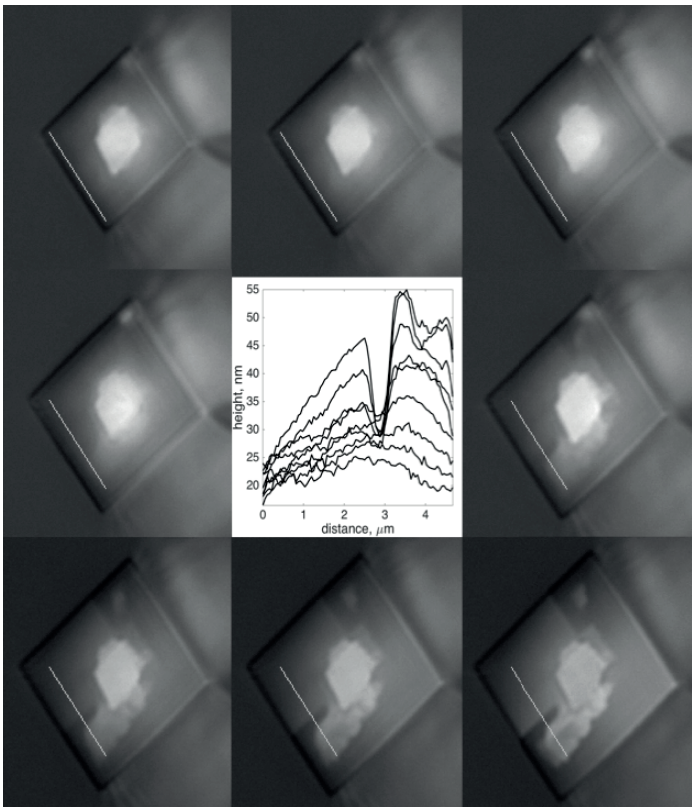

Figure 7. Evolution from smooth to rough growth rim for Crystal H at Ω = 0.6. The images are 10 × 12 μm, and the time between images is 6 min. The figure shows height profiles along the white line in the images demonstrating how the initially smooth, flat surface develops a "protrusion" pushing the crystal up and tilting it.

3.2. Summary of Growth Rates

Table 1 summarizes the growth rates of all the crystals presented in this paper. There is a large variation in growth rates both vertically and outwards at nominally identical conditions. The ratio of the vertical to the outwards growth rates shows that the confined surfaces of crystals that grow in an intermittent fashion grow consistently faster than the smooth contacts (100 $dz/dr \approx 13\%$ for intermittent and from 7% down to 0% for smooth contacts). Smooth contacts also tend to slow down or stop growing upwards after a certain time. In a recent, similar study, we find, for $NaClO_3$, dz/dr to be about 16% on average [25].

Table 1. Summary of growth rates for all the crystals. "Downward growth rate" is the growth rate in the confined region causing the crystal to be lifted upwards.

Crystal	Concentration c mM	Supersaturation	Downward Growth Rate $v = dz/dt$ nm/h	Smooth/ Intermittent	Outwards Growth Rate dr/dt nm/h	Relative Growth Rate $100 \times dz/dr$ %
A	0.8	0.6	$19 \rightarrow 1.1$	Smooth	310 ± 9	$(6\rightarrow)0.4$
B	0.7	0.4	180 ± 5	Rough	850 ± 10	21
C	0.8	0.6	$114 \rightarrow 0$	Smooth	1430 ± 70	$8(\rightarrow)0$
D	0.7	0.4	15 ± 1	Smooth	290 ± 30	5
E	0.8	0.6	31 ± 1	Rough	250 ± 20	12
F	0.8	0.6	$6 \pm 1 \rightarrow 0$	Smooth	190 ± 30	$(3\rightarrow)0$
G	0.7	0.4	$15 \rightarrow 3$	Smooth	130 ± 20	$(12\rightarrow)3$
H	0.8	0.6	77 ± 5	Rough	1240 ± 50	6

4. Discussion

4.1. Disjoining Pressure: The Hovering Crystal

For Crystal A, we calculated the stress at the contact $P = F/A_c = r^2(\rho_c - \rho_s)g/(2w)$. Using this calculation for the widths shown in Figure 2D and using Equation (1) and the corresponding intensities, we may calculate the disjoining pressure versus fluid film thickness, h. As mentioned, the absolute value of the calculated fluid film thickness has an uncertainty of about ± 10 nm due to the uncertainty of determining the minimum intensity of the closest contact.

In order to check whether this range of pressures (0.14–2.42 Pa) can be sustained by the disjoining pressure of a fluid film, we have calculated disjoining pressures using the DLVO theory for silica-calcite. We have used Equation (S4) from Diao and Espinosa-Marzal [26] and their parameters for a saturated $CaCO_3$ solution (0.51 mM Ca^{2+}) (Tables S1 and S3 in [26]), as well as the Hamaker constant computed by their Equation (S3). The resulting curve in Figure 8 shows the disjoining pressure for silica (calcite together with the pressure) distance data from our experiment. This shows that our stress-distance measurements coincide surprisingly well with the disjoining pressures from DLVO theory. This signifies that as the the width of the growth rim changes (as shown in Figure 2), the change in area of contact and corresponding contact pressure causes the crystal to hover up and down as the fluid film thickness adjusts to where the disjoining pressure balances the contact pressure.

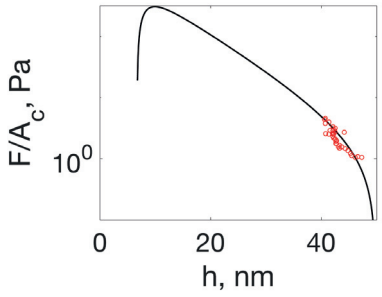

Figure 8. Disjoining pressure of silica on calcite interface in saturated $CaCO_3$ solution calculated from DLVO theory (whole drawn line) and contact pressures versus fluid film thickness, h, calculated from experimental interference intensities for Crystal A.

4.2. Smooth and Rough Contacts

The distribution of fluid film thicknesses in Figure 6 is quite remarkable when compared to the disjoining pressure and fluid film thicknesses of Crystal A shown in Figure 8. Over time, about 1/3 of the growth rim of Crystal B has a fluid film thickness, h, less than 50 nm and therefore experiences a

non-negligible disjoining pressure. Two thirds of the growth rim are not affected by disjoining pressure and have a larger "gap" to allow more diffusion of ions to the growth rim surface spreading over a larger width w. There is a peak in the distribution at around 25 nm where the disjoining pressure is about 10-times larger than the disjoining pressure that keeps Crystal A (with a smooth rim) hovering above the glass surface. It is easily understandable that a smaller surface carrying the same load needs to sustain a larger pressure.

The rough profiles of the growth rim that we observe in Figure 5 are very similar to the profiles of growth rims measured ex situ by Røyne and Dysthe [11] on $NaClO_3$ crystals (see Figures 3 and 4 in [11]). These crystals were typically 100-times larger than the $CaCO_3$ crystals in this study, and the differences in height along the growth rim were up to 10 μm, which is 50-times larger than on Crystal B.

What is the cause of some crystals developing a rough contact?

1. Dislocations? In some cases, there seems to be growth resembling (atomic) step spirals emanating from larger steps on the surface. However, the fact that the macroscopic steps on the growth rim move around does not match with a screw dislocation normal to the surface.
2. Local poisoning of growth by "dirt", asperities on the glass surface or organic molecules from the PDMS? We have no evidence that the solutions or the PDMS are different in the experiments of smooth vs. rough growth rims. Sometimes, we have observed smooth and rough growth rims on crystals adjacent to each other in the same experiment like Crystals E and F (see the images in the Supplementary Materials). If a surface active contamination adheres to the growing surface, it is likely to be incorporated in the crystal when it continues growing. Then, there would have to be a continuous addition of contamination for rough crystals to keep them rough and no contamination for smooth crystals. If the "contamination" adheres to the glass surface, it would be a constant source of "disturbance" at a fix point in space.
3. An inherent transport–growth instability induced by nanoconfinement? The fact that similar roughness is found on growth rims of otherwise perfectly faceted crystals of sodium chlorate [11], potassium alum [16] and calcite (this study) suggests that this is a general nonlinearity/transport–growth feedback mechanism in confinement that arises from random perturbations, be they local contamination, roughness of the support or something else. We have yet to pinpoint the nature of the feedback mechanism and formulate a mathematical model for it.

4.3. Rim Widths of Smooth Rims

In the special case of smooth rims, we may use a simple mass balance argument for the width of the growth rim. Outside the crystal, the ion concentration, c, is held constant. Since there is no growth inside the growth rim, we assume that the concentration there as well is constant, $c = c_0$. In order to maintain these conditions, the diffusive current of ions from the solution into the confined fluid film must equal the current of ions to the surface due to growth of the growth rim:

$$-D\frac{dc}{dx}h = \rho w v \tag{3}$$

where D is the diffusion coefficient of the ions in the confined fluid, w is the width of the growth rim, h is the thickness of the fluid film and v is the vertical growth rate of the rim. This leads to a relation for the width of a growth rim:

$$w^2 = \frac{2h}{v}\frac{Dc_0}{\rho}\Omega \tag{4}$$

where the first fraction comprises the experimental observables, the second fraction (diffusion coefficient and ratio of solid and liquid densities) is specific to the crystal and $\Omega = (c - c_0)/c_0$ is the dimensionless imposed supersaturation. Crystals A, D and G are examples of smooth crystals with vertical growth rates of 20–25 nm/h before the fluid film diminishes and the vertical growth stops. The ratio β:

$$\beta = \sqrt{\frac{2h}{v}\frac{Dc_0}{\rho}\Omega}/w \tag{5}$$

equals one for the theoretical prediction. If we use numbers for Crystal A ($v = 7 \times 10^{-12}$ m/s, $\Omega = 0.6$, $Dc_0/\rho = 9 \times 10^{-14}$ m^2/s and $h/w^2 = 2000$–4000 m^{-1}), the ratio $\beta = 5$–8. Recent experiments on the ionic crystal $NaClO_3$, which has a solubility c_0 more than 1000-times larger than $CaCO_3$, show that the ratio $\beta = 1$–2 depending on the diffusion coefficient used [25]. This means that although the growth rates are a factor 1000 different and w is around 100 μm for $NaClO_3$ and 4 μm for $CaCO_3$, the ratio between the expected rim-widths is only $\beta_{CaCO_3}/\beta_{NaClO_3} = 4$–$5$. This means that the mass balance argument for predicting rim widths is reasonable even when solubilities and growth rates vary by many orders of magnitude. It should be noted that we have used the bulk diffusion coefficients. We know that diffusion slows down as the fluid film gets thinner, but this does not give significant reduction in the diffusion coefficient for fluid film thicknesses larger than 10 nm [21,27]. A smaller diffusion coefficient in the fluid film will give a smaller β.

4.4. Rim Widths of Rough Rims

As a comparison, we may also calculate β for Crystal B using the fluid film thickness in contact, $h = 25$ nm, growth rim width, $w = 0.5$–2 μm, and vertical growth rate, $v = 185$ nm/h, yielding $\beta = 2.5$–10. This result, that the ratio β is the same for $CaCO_3$ independent of growth mode, may be a hint of where to find the explanation for the different growth modes. β only tells us there should be a balance of fluxes relating h, w and v, but it says nothing about which w (or which h) the crystal should choose. The force on the confined interface at any time is given and is related to the contact area and pressure in the contact: $F = Pw_c l_c$, where w_c is the contact width and l_c is the length of the contact area. The disjoining pressure in the range $h = [10, 60]$ nm can be simplified to $P = \alpha e^{-h/h_0}$, where $\alpha = 3000$ Pa and $h_0 = 20$ nm. Combining these two expressions, we get a relation for the mechanical stability of the contact relating w and h:

$$w = \frac{Fe^{h/h_0}}{\alpha l_c} \tag{6}$$

Combining this with Equation (4) gives a relation between the growth rate and the fluid film thickness:

$$v = \frac{Dc_0\Omega}{\rho}\left(\frac{\alpha l_c}{F}\right)^2 2he^{-2h/h_0} \tag{7}$$

which has a maximum for $h = h_0/2 = 10$ nm. This is inside the first peak in the fluid film width distribution in Figure 8. This is a surprising result, because intuition tells us that the vertical growth should increase with fluid film thickness h because there is more room for diffusion of ions into the contact. The positive feedback yielding a maximum is due to the fact that the ions diffusing in a thinner film distribute over a narrower contact width.

There is no fundamental reason why a system should choose the highest growth velocity. In fact, we see two types of development: smooth contacts where the vertical growth stops and smooth contacts where some perturbation in the form of a dislocation changes the growth dynamics locally. Any such perturbation leading to a film thickness h closer to $h_0/2$ will tend to make this part of the crystal grow faster vertically. The contact area growing at maximum speed will outpace the rest of the crystal rim. The next question is then: why are these areas of contact not stable in the sense that they persist at growing faster than the rest of the crystal? Probably, the lower growth rate at $h < 10$ nm prevents the closest contacts from "running away" from the rest of the growth rim.

The much faster vertical growth rate of Crystal B (see Figure 3) may thus be explained by the smaller distance h between the contact part of the growth rim and the glass. The observation we have not yet accounted for is why the contact regions move around (see Figure 5) and the crystal tilts this way and that causing the crystal to "wobble" its way up at a remarkably steady pace (see Figure 4).

5. Conclusions

5.1. Summary of Main Results

By combining high stability flow microfluidics and quantitative reflection interference contrast microscopy (RICM), we have been able to grow calcite crystals in a defined region permitting high resolution microscopy, obtaining a high degree of control of solution supersaturation, to measure the growth rates on the free surfaces and at the confined surface of the crystal, to measure quantitatively the topography of the confined crystal surface, to measure the thickness of the fluid film confined between the crystal and the glass support and to quantify a number of novel aspects of confined crystal growth.

Confinement of crystals growing from solution induces transport limitations on the mass flux to the growing crystal surface. The first result of this limitation is the appearance of a cavity where no growth occurs, and an outer rim where growth occurs, causing the crystal to be pushed away from the confining surface.

The growth at the confined growth rim depends on the existence and thickness of a fluid film confined between the crystal and the glass support. The thickness of this fluid film is shown to change with pressure as predicted by the DLVO theory.

We have observed and quantified in situ two main growth modes of confined crystal growth for $CaCO_3$ that have also been observed ex situ for $NaClO_3$: smooth growth rims and rough, intermittently growing growth rims. The smooth rims are flat compared to the vertical resolution of our measurement technique (a few nm). The vertical growth rate of smooth rims tends to slow down with time and crystal size.

Our measurements of the growth rim width and area of contact for smooth rims are consistent with a mathematical model and with the width of growth rims of $NaClO_3$ crystals that are 10,000-times more soluble than $CaCO_3$.

The rough rims have small regions of load bearing contact and larger regions of larger fluid film thickness. The regions of load bearing contacts move around the growth rim, and the growth velocity at any point on the rim is intermittent. This causes a "wobbling" vertical motion of the crystal. The vertical speed is much higher than that of the crystals with smooth growth rims. The instability causing the transition from smooth to rough is not yet understood.

5.2. Outlook

This study shows that confined crystals grow at the outer rim and that this growth rim may be smooth as predicted by Weyl [10] and by a simple model or it may become rough, dynamic, intermittently growing and with an area of contact that is not easily measured. The contact stresses for both the smooth and rough rims agree with disjoining pressure from the DLVO theory. Both smooth rim widths and rough rim topography agree with results for sodium chlorate [11]. This signifies that the phenomena presented here are general for crystal growth in nanoconfinement and not limited to calcite. We have presented strong evidence that the transition from smooth to rough is a generic confinement-induced instability. The results presented here should be a good base for formulating and testing mathematical models of this instability. Such a mathematical model is necessary to understand how crystals of different sizes grow when confined by different surfaces. We need to understand the instability documented here if we are to answer the general question "when does crystallization in confinement lead to stress buildup and damage, and when does crystallization cease due to confinement?" Experiments revealing interface topography at much higher stresses, approaching the thermodynamic limit, will also be necessary to answer this question.

Supplementary Materials: The following are available online at www.mdpi.com/2073-4352/7/12/361/s1: Videos CrystalA.avi and CrystalB.avi and a file with images of the other crystals for which we have presented results. Figure S1: Thirteen hours of growth of Crystal C. The Ca^{2+} concentration here was 0.8 mM. Flow direction from bottom to top; Figure S2: Sixteen hours of growth of Crystal D. The Ca^{2+} concentration here was

0.7 mM. Flow direction from bottom to top; Figure S3: Nineteen hours of growth of Crystals E and F. The Ca^{2+} concentration here was 0.7 mM. This experiment shows the two classes of confined crystal contacts at the same time: intermittent (top) and smooth (bottom). Flow direction from bottom to top; Figure S4: Twenty five hours of growth of Crystal G. The Ca^{2+} concentration here was 0.7 mM. Flow direction from left to right. The confined contact surface is not a $10\bar{1}4$ surface; Figure S5: Four hours of growth of Crystal H. The Ca^{2+} concentration here was 0.7 mM. The crystal seems initially smooth and flat. After 1 h, it develops a "defect" and continues to grow two separate flat surfaces at different heights, and the crystal surface tilts with respect to the glass surface. Flow direction from bottom to top.

Acknowledgments: This project has received funding from the European Union's Horizon 2020 research and innovation program under the Marie Sklodowska-Curie Grant Agreement No. 642976 (ITN NanoHeal) and from the Norwegian Research Council Grant No. 222386.

Author Contributions: Lei Li designed and performed the experiments, analyzed the data and contributed to writing the paper. Dag Kristian Dysthe conceived of and designed the experiments, analyzed the data and wrote the paper. Anja Røyne and Felix Kohler contributed to the analysis of the data and writing the paper.

Conflicts of Interest: The authors declare no conflict of interest.

Abbreviations

The following abbreviations are used in this manuscript:

RICM	Reflection interference contrast microscopy
PDMS	Polydimethylsiloxane
PGMEA	Propylene glycol methyl ether acetate
LED	Light-emitting diode

References and Notes

1. Wilkinson, B.H. Biomineralization, paleoceanography, and the evolution of calcareous marine organisms. *Geology* **1979**, *7*, 524–527.
2. Stephens, C.J.; Ladden, S.F.; Meldrum, F.C.; Christenson, H.K. Amorphous Calcium Carbonate is Stabilized in Confinement. *Adv. Funct. Mater.* **2010**, *20*, 2108–2115.
3. Gratier, J.-P.; Dysthe, D.K.; Renard, F. The role of pressure solution creep in the ductility of the Earth's upper crust. *Adv. Geophys.* **2013**, *54*, 47–179.
4. Flatt, R.J.; Caruso, F.; Sanchez, A.M.A.; Scherer, G.W. Chemo-mechanics of salt damage in stone. *Nat. Commun.* **2014**, *5*, 4823.
5. Chang, C.F.; Chen, J.W. The experimental investigation of concrete carbonation depth. *Cem. Concr. Res.* **2006**, *36*, 1760–1767.
6. Rothrock, E.P. On the force of crystallization of calcite. *J. Geol.* **1925**, *33*, 80–83.
7. Gratier, J.P.; Frery, E.; Deschamps, P.; Røyne, A.; Renard, F.; Dysthe, D.; Ellouz-Zimmerman, N.; Hamelin, B. How travertine veins grow from top to bottom and lift the rocks above them: The effect of crystallization force. *Geology* **2012**, *40*, 1015–1018.
8. Gibbs, J.W. *Scientific Papers of J. Willard Gibbs, Volume 1: Thermodynamics*; Longmans, Green and co.: Harlow, UK, 1906.
9. Correns, C.W. Growth and dissolution of crystals under linear pressure. *Discuss. Faraday Soc.* **1949**, *5*, 267–271.
10. Weyl, P.K. Pressure solution and the force of crystallization: A phenomenological theory. *J. Geophys. Res.* **1959**, *64*, 2001–2025.
11. Røyne, A.; Dysthe, D.K. Rim formation on crystal faces growing in confinement. *J. Cryst. Growth* **2012**, *346*, 89–100.
12. Espinosa-Marzal, R.M.; Scherer, G.W. Advances in understanding damage by salt crystallization. *Acc. Chem. Res.* **2010**, *43*, 897–905.
13. Noiriel, C.; Renard, F.; Doan, M.L.; Gratier, J.P. Intense fracturing and fracture sealing induced by mineral growth in porous rocks. *Chem. Geol.* **2010**, *269*, 197–209.
14. Wheeler, J. Dramatic effects of stress on metamorphic reactions. *Geology* **2014**, *42*, 647–650.
15. Schmalholz, S.M.; Podladchikov, Y. Metamorphism under stress: The problem of relating minerals to depth. *Geology* **2014**, *42*, 733–734.
16. Becker, G.F.; Day, A.L. The linerar force of growing crystals. *Proc. Wash. Acad. Sci.* **1905**, *7*, 283–288.

17. Taber, S. The growth of crystals under external pressure. *Am. J. Sci.* **1916**, *41*, 532–556.
18. Flatt, R.J.; Steiger, M.; Scherer, G.W. A commented translation of the paper by C.W. Correns and W. Steinborn on crystallization pressure. *Environ. Geol.* **2007**, *52*, 221–237.
19. It should be noted that Correns stated that sodium chlorate did not crystallize in confinement to produce work, whereas Røyne and Dysthe [11] did measure such work, although the rates of growth were very small. It is also worth noting that all studies before Røyne and Dysthe [11] were performed using hydrated salts, while sodium chlorate, as calcite in this study, does not consist of hydrated salts.
20. Israelachvili, J.N. *Intermolecular and Surface Forces*; Academic Press: Cambridge, MA, USA, 2011; p. 674.
21. Dysthe, D.K.; Renard, F.; Porcheron, F.; Rousseau, B. Fluid in mineral interfaces—Molecular simulations of structure and diffusion. *Geophys. Res. Lett.* **2002**, *29*, 13–14.
22. Li, L.; Sanchez, J.R.; Kohler, F.; Røyne, A.; Dysthe, D.K. Microfluidic control of nucleation and growth of calcite. *arXiv* **2017**, arXiv:1708.06299.
23. Ploem, J.S. Reflection-contrast microscopy as a tool for investigation of the attachment of living cells to a glass surface. In *Mononuclear Phagocytes in Immunity, Infection and Pathology*; Furth, R.V., Ed.; Blackwell Scientific Publications: Oxford, UK, 1975; pp. 405–421.
24. The value of h depends on an estimate of the minimum intensity attainable in the contact and the maximum value recorded for the constructive interference, and we consider the accuracy to be about ± 10 nm. The dependence of h on intensity is more accurate because the total intensity range has an accuracy better than 10%. This means that the height data in Figure 2 is accurate to ± 10 nm, and the slope that these points form (dP/dh in Figure 2) is accurate to 10%.
25. Kohler, F.; Dysthe, D.K.; Gagliardi, L.; Pierre-Louis, O. Cavity formation in confined growing crystals. *Phys. Rev. Lett.* **2017**, under review.
26. Diao, Y.; Espinosa-Marzal, R.M. Molecular insight into the nanoconfined calcite-solution interface. *Proc. Natl. Acad. Sci. USA* **2016**, *113*, 12047–12052.
27. Using the data in Dysthe et al. [21], the diffusion coefficient in a confined fluid film of thickness h is $D(h) = D(h = \infty)(1 - e^{-h/h_0})$, where $h_0 = 5.6$ nm.